Cell Reports

Resource

Reprogramming Bacteriophage Host Range through Structure-Guided Design of Chimeric Receptor Binding Proteins

Graphical Abstract

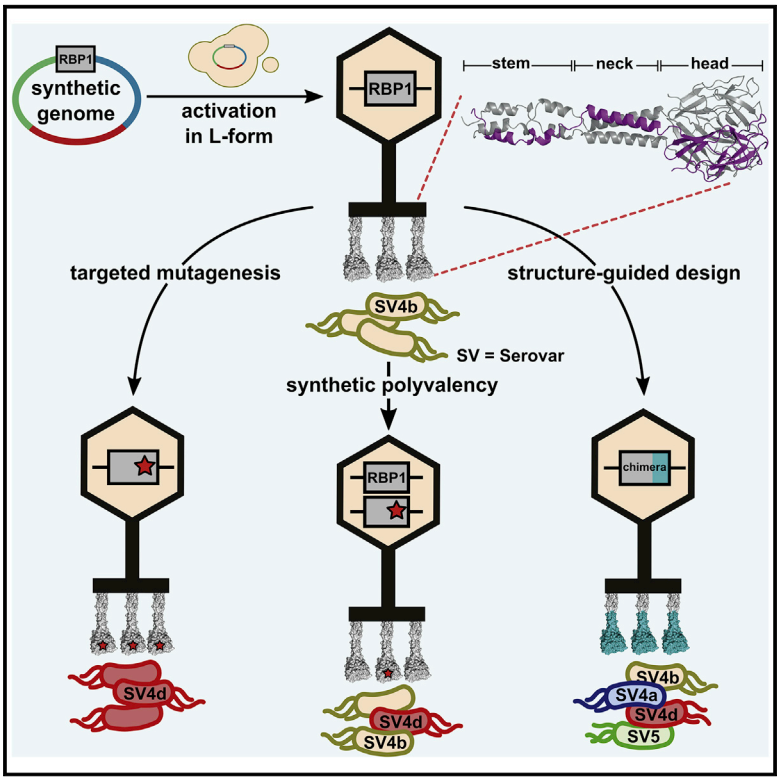

Authors

Matthew Dunne, Beatrice Rupf, Marc Tala, ..., Andreas Plückthun, Martin J. Loessner, Samuel Kilcher

Correspondence

samuel.kilcher@hest.ethz.ch

In Brief

Receptor binding proteins (RBPs) are key determinants of bacteriophage host range. Dunne et al. solve the RBP crystal structure of *Listeria* phage PSA and combine synthetic biology with structure-guided approaches to re-program RBP specificity. Using the temperate, narrow host range PSA scaffold, they construct virulent phages with extended and defined host specificities.

Highlights

- Adaptation of *Listeria* phage serovar specificity through targeted RBP variations
- High-resolution crystal structure of a *Listeria* phage receptor binding protein
- Structure-guided design of RBP chimeras yields phages with predictable host ranges
- Synthetic RBPs extend phage binding specificity (from SV 4b to 4a, 4b, 4d, 5, 6b)

Dunne et al., 2019, Cell Reports *29*, 1336–1350
October 29, 2019
https://doi.org/10.1016/j.celrep.2019.09.062

CellPress

OPEN ACCESS
CellPress

Cell Reports
Resource

Reprogramming Bacteriophage Host Range through Structure-Guided Design of Chimeric Receptor Binding Proteins

Matthew Dunne,[1] Beatrice Rupf,[1] Marc Tala,[1] Xhem Qabrati,[1] Patrick Ernst,[2] Yang Shen,[1] Eric Sumrall,[1] Laura Heeb,[1] Andreas Plückthun,[2] Martin J. Loessner,[1] and Samuel Kilcher[1,3,*]
[1]Institute of Food Nutrition and Health, ETH Zurich, Zurich, Switzerland
[2]Department of Biochemistry, University of Zurich, Zurich, Switzerland
[3]Lead Contact
*Correspondence: samuel.kilcher@hest.ethz.ch
https://doi.org/10.1016/j.celrep.2019.09.062

SUMMARY

Bacteriophages provide excellent tools for diagnostics, remediation, and targeted microbiome manipulation, yet isolating viruses with suitable host specificity remains challenging. Using *Listeria* phage PSA, we present a synthetic biology blueprint for host-range engineering through targeted modification of serovar-specific receptor binding proteins (RBPs). We identify Gp15 as the PSA RBP and construct a synthetic phage library featuring sequence-randomized RBPs, from which host range mutants are isolated and subsequently integrated into a synthetic, polyvalent phage with extended host range. To enable rational design of chimeric RBPs, we determine the crystal structure of the Gp15 receptor-binding carboxyl terminus at 1.7-Å resolution and employ bioinformatics to identify compatible, prophage-encoded RBPs targeting different *Listeria* serovars. Structure-guided design enables exchange of heterologous RBP head, neck, or shoulder domains to generate chimeric phages with predictable and extended host ranges. These strategies will facilitate the development of phage biologics based on standardized virus scaffolds with tunable host specificities.

INTRODUCTION

Modulation of microbiomes through targeted therapeutic intervention is an important avenue of drug development (McCarville et al., 2016; Schmidt et al., 2018). Bacteriophages are highly suitable for this purpose because they recognize their target bacteria with unmatched specificity, a property that is mediated by receptor binding proteins (RBPs). These proteins are key determinants of the taxonomic diversity that a given phage can target, i.e., the phage host range (de Jonge et al., 2019). In addition to their specificity, phages deliver genetic information and have the potential to remove selected species without affecting the overall microbiome composition. With recent progress in phage engineering techniques (Ando et al., 2015; Kilcher et al., 2018), the development of customized phage vectors for targeted microbiome intervention seems to be achievable (Kilcher and Loessner, 2019). For example, several studies have demonstrated that targeted phage vectors can be utilized to re-sensitize or remove antibiotic-resistant bacteria from mixed populations (Bikard et al., 2014; Citorik et al., 2014; Edgar et al., 2012; Goren et al., 2017; Yosef et al., 2015).

The ability of phages to bind target bacteria with species and sub-species specificity is their greatest virtue, but at the same time a significant limitation: host ranges of isolated phages are frequently too narrow or do not match the requirements for a specific application. This limitation will become even more evident when moving from model systems to clinical application. To this date, phages with suitable specificity have to be identified from environmental isolates, which is a time- and cost-intensive process (Nilsson, 2014; Schmidt, 2019). Often, these isolates are subsequently combined to produce "phage cocktails" with the desired host range (Gordillo Altamirano and Barr, 2019). Because phages are extremely diverse in structure and genetic composition, each isolate or cocktail component must be sequenced and properly characterized before it can be used safely in a medical application (Philipson et al., 2018). To circumvent these issues, it may be possible to engineer a limited number of well-characterized phages to bind and infect the strains of interest (Ando et al., 2015). However, this approach requires an in-depth molecular understanding of RBP-host interactions, which is often lacking (de Jonge et al., 2019).

Host range modification of some phages has been achieved, most often through exchange of C-terminal domains within tail-fiber genes of closely related virulent phages, such as members of the T7, T4, and T2 families (Ando et al., 2015; Chen et al., 2017; Le et al., 2013; Mahichi et al., 2009; Pouillot et al., 2010; Trojet et al., 2011; Yoichi et al., 2005; Yosef et al., 2017). For siphoviruses (double-stranded DNA [dsDNA] phages with flexible tails), host range modification is particularly difficult, because their RBPs (also known as tail spikes) are an integral part of the baseplate; i.e., the phage adsorption and DNA delivery apparatus. As such, tail spikes are involved in multiple protein-protein interactions within the baseplate. Modification of tail spike sequences can affect the overall integrity of this macromolecular complex, ultimately impeding the formation of infectious virions. Unsurprisingly, only a few reports describe host range modification

Table 1. Engineered Phages with Modified Host Range Constructed in This Study

Bacteriophage Genotype	Acquired *Listeria* SV Specificity						Shift/Expand	Engineering Step	Reference
	4a	4b	4c	4d	5	6b			
PSA	–	++	–	–	–	–	nA	nA	Zimmer et al., 2003
PSA ΔLCR *ply511*	–	++	–	–	–	–	nA	LCR deletion, *ply511* addition	Kilcher et al., 2018
PSA ΔLCR *ply511 gp15*_S302R	–	+	–	++	–	–	shift	isolate from phage RBP library	this study
PSA ΔLCR *ply511 gp15*_S306K	–	+	–	++	–	–	shift	isolate from phage RBP library	this study
PSA ΔLCR *ply511 gp15*_S306R	–	+	–	++	–	–	shift	isolate from phage RBP library	this study
PSA ΔLCR *ply511 gp15*_A332V	–	+	–	++	–	–	shift	isolate from phage RBP library	this study
PSA ΔLCR *ply511 gp15*_S334R	–	+	–	++	–	–	shift	isolate from phage RBP library	this study
PSA ΔLCR *ply511* $gp15_{CO}$_S334R	–	+	–	++	–	–	shift	isolate from phage RBP library	this study
PSA ΔLCR *ply511 gp15*_S354T	–	+	–	++	–	–	shift	isolate from phage RBP library	this study
PSA ΔLCR *ply511 gp15*_WT $gp15_{CO}$_S334R	–	++	–	++	–	–	expansion	RBP duplication + modification	this study
PSA ΔLCR *ply511* stem chimera L99	++	+	–	+	+	–	expansion	chimeric RBP (stem)	this study
PSA ΔLCR *ply511* neck chimera L99	++	+	–	+	+	–	expansion	chimeric RBP (neck)	this study
PSA ΔLCR *ply511* stem chimera ATCC35897	+	++	–	+	++	(+)	expansion	chimeric RBP (stem)	this study
PSA ΔLCR *ply511* stem chimera WSLC30151	+	+	–	+	++	(+)	expansion	chimeric RBP (stem)	this study
PSA ΔLCR *ply511* neck chimera WSLC30151	+	+	–	+	++	(+)	expansion	chimeric RBP (neck)	this study

++, high eop; +, reduced eop; (+), lysis zones observed in spot assays; –, no infection; SV, serovar.

through exchange of tail spike domains (Duplessis and Moineau, 2001; Kot et al., 2013; Vegge et al., 2006). Without structural information, these approaches depend on the availability of RBP sequences from very similar phages with distinct host range.

Platform technologies that enable more systematic host-range programming through exchange of specificity determinants have previously been established for phages that infect Gram-negative bacteria (Ando et al., 2015; Yosef et al., 2017; Yehl et al., 2019). So far, these approaches are limited to T7-like podoviruses, whose host specificity is primarily determined by the tail-fiber protein Gp17 (Molineux, 2006). These landmark studies demonstrated the ability to systematically modulate and extend the host range of T7-like phages for productive infection (Ando et al., 2015; Yehl et al., 2019) and DNA transduction (Yosef et al., 2017) of Enterobacteriacea. These approaches depend on the generation of chimeric particles with heterologous tail fibers or tail structures. For all other phage families, particularly those targeting Gram-positive pathogens, such engineering platforms are not yet available.

In this study, we outline several synthetic biology strategies for host-range modification that are based on gene diversification, pathogen-specific RBP database searches, and the construction of phages with chimeric baseplates. As such, these approaches do not depend on the availability of isolated, well-characterized phages with a suitable host range. Using *Listeria monocytogenes* as a model, we demonstrate that synthetic, strictly lytic phages with extended host ranges can be constructed based on a very narrow-range temperate virus. These strategies can be directly applied to synthesize phages targeting other important Gram-positive pathogens. An overview of all synthetic phages constructed in this study is provided in Table 1.

RESULTS

Gp15 Is the RBP of Phage PSA and Recognizes Galactosylated Wall Teichoic Acid

Most phages of the genus *Listeria* bind to cell wall-anchored anionic glycopolymers, termed wall teichoic acids (WTAs) (Dunne et al., 2018b). There is a large degree of structural diversity within *Listeria* WTAs (Shen et al., 2017), which also serve as the major antigenic determinant underlying the O-antigen of the *Listeria* serotyping scheme (Kamisango et al., 1983). Therefore, most *Listeria* phages feature serovar-specific infection patterns (Dunne et al., 2018b). *Listeria* WTAs are polymeric ribitol-phosphate (RboP) chains directly linked to peptidoglycan via a linkage unit. They are subdivided into two types; type I RboP units are directly linked to each other via a phosphodiester bond, whereas type II RboP units are connected via an integrated N-acetylglucosamine (GlcNAc) (Shen et al., 2017). Additionally, WTA RboP repeating units can be decorated with rhamnose, glucose, galactose, or GlcNAc, and can be O-acetylated (Uchikawa et al., 1986) (see Figure 1A for an overview). These glycosidic decorations define the different *Listeria* serovars. Because of the structural diversity between serovars, most *Listeria* strains escape phage predation by modifying their WTA glycosylation patterns, rather than by employing intracellular defense mechanisms (Eugster et al., 2015). Only few *Listeria* phages infect a broad range of serovars, and they are likely polyvalent, i.e., use

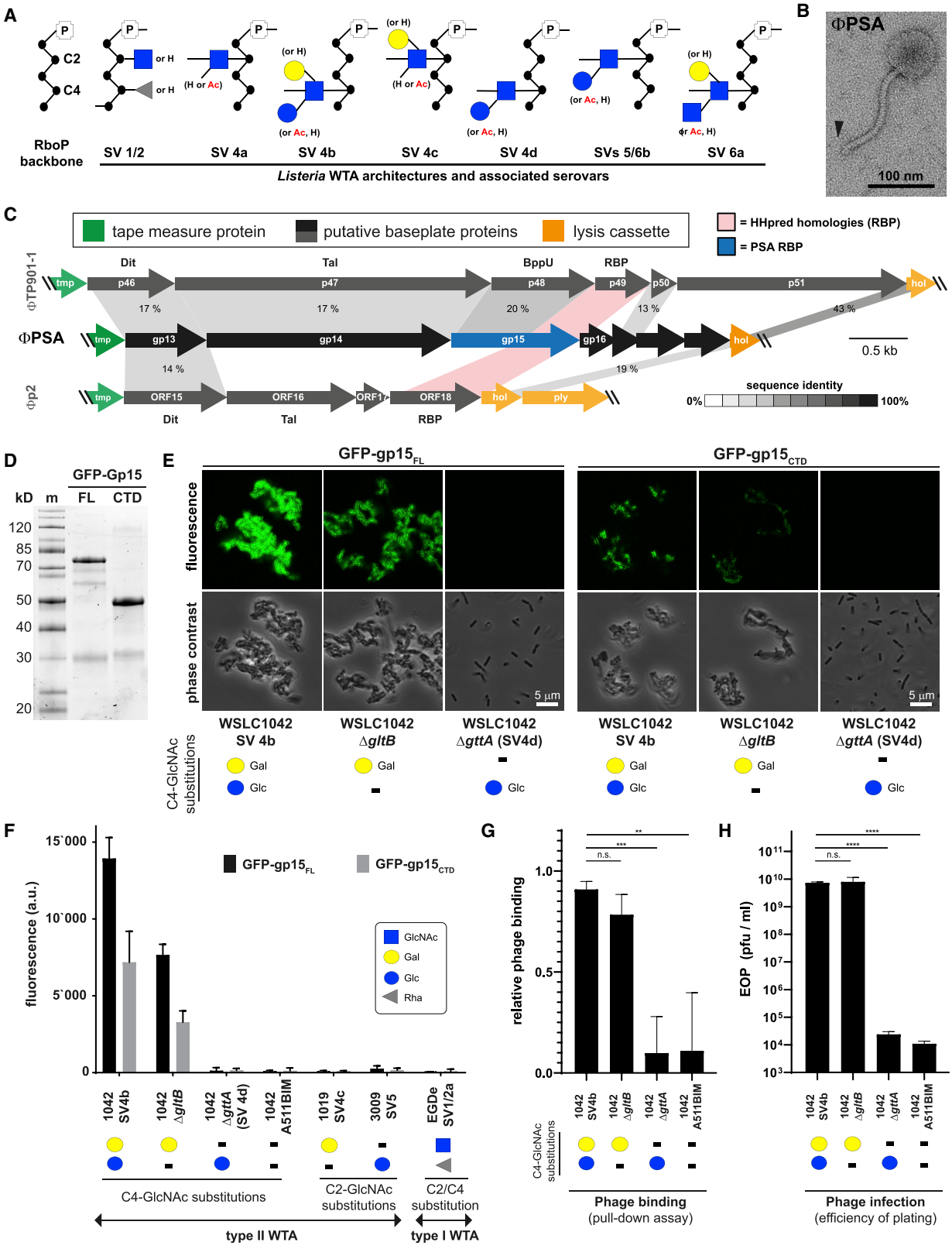

(legend on next page)

multiple RBPs for recognizing different receptors (Habann et al., 2014; Wendlinger et al., 1996).

Here, we used a temperate phage harbored by *L. monocytogenes* strain ScottA (PSA) as a model for host-range programming, because this siphovirus (see electron micrograph in Figure 1B) features a very narrow host range, restricted to serovar (SV) 4b *Listeria* strains (Loessner et al., 1994; Zimmer et al., 2003). Most siphoviruses encode their baseplate-morphogenesis modules between the tail tape measure protein and the lysis cassette (holin and endolysin; Dunne et al., 2018b). To identify the PSA RBP, we analyzed the genes within this submodule (*gp13* to *gp19*) using HHpred protein homology detection and structure prediction (Söding et al., 2005). This analysis revealed structural similarities between the C-terminal domain of PSA Gp15 and the RBPs of *Lactococcus* phages TP901-1 and p2 (Table S1). Structural similarity between *Listeria* and *Lactococcus* phages seems to be common and has previously been observed (Cambillau, 2015; Dupuis and Moineau, 2010). Based on sequence similarity and gene synteny, the PSA baseplate is partially related to the TP901-1 adsorption apparatus (Figure 1C). We expressed and purified GFP-gp15 fusion proteins using the full-length and C-terminal domain (amino acids 201–373) of the PSA RBP candidate (GFP-gp15$_{FL}$ and GFP-gp15$_{CTD}$) (Figure 1D). Both proteins bind the surface of SV 4b cells (*L. monocytogenes* strain WSLC1042), as revealed by confocal microscopy and spectrophotometric binding assays (Figures 1E and 1F). Despite quantitative differences in cell decoration between full-length (FL) and C-terminal domain (CTD), positive binding by GFP-gp15$_{CTD}$ revealed that the C terminus confers receptor binding. The observed bacterial aggregation (Figure 1E, phase contrast) indicates the presence of multiple binding domains within a functional RBP unit, a feature typically observed for other phage RBPs (Dunne et al., 2018b). SV 4b cells feature type II WTA whose RboP units are connected at the C4 position via an integrated GlcNAc moiety (see cartoons in Figure 1A). This GlcNAc is further glucosylated, galactosylated, and O-acetylated (Shen et al., 2017). Using glycosylation mutants that lack either glucose (WSLC1042 *ΔgltB*), galactose (WSLC1042 *ΔgttA*), or both (WSLC1042_A511-BIM) (Sumrall et al., 2019), we found that RBP binding strictly depends on the presence of galactose and thus identified galactosylated GlcNAc as the carbohydrate receptor of the RBP of phage PSA (Figures 1E and 1F). Galactosylation of GlcNAc was not only strictly required for Gp15 binding, but also for phage adsorption (Figure 1G) and plaque formation (Figure 1H), suggesting it serves as the functional phage receptor *in vivo*. In contrast, the glucose decoration was not required for cell wall recognition, phage adsorption, or phage infection (Figures 1F–1H); however, when glucose was removed from the WTA, the relative amount of cell decoration by GFP-RBPs is halved (Figure 1F), suggesting glucose substitutions are a non-essential but beneficial constituent of the RBP receptor epitope. Interestingly, SV 4c cells (WSLC1019) are not bound by GFP-gp15$_{FL}$ or GFP-gp15$_{CTD}$ (Figure 1F). The only difference between SVs 4b and 4c is the C2 connectivity of the latter (see Figure 1A), demonstrating that the PSA RBP is specific for galactosylated GlcNAc at the RboP C4 position. In sum, we have identified Gp15 as the PSA RBP and demonstrate its ability to differentiate type II WTAs based on the presence or absence of a single galactose at the C4 position of the RboP repeating unit. This suggests that the specificity of the Gp15 C terminus confers the narrow host range of this temperate phage.

RBP-Specific Sequence Diversification Produces Phage Mutants with Shifted Host Range

To generate PSA derivatives with modified host ranges, we developed a workflow based on targeted diversification of PSA *gp15*, which does not introduce mutations within the rest of the phage genome and thus limits host-range adaptations to RBP mutants (Figure 2A). In addition to binding a novel host, we had to ensure the host range mutants were plaque-forming, virulent phages capable of injecting DNA, replicating within the host, and releasing progeny through endolysin cell lysis. We therefore used the previously engineered PSA derivative (PSA ΔLCR *ply511*) as a backbone, which contains two genetic modifications: First, an additional endolysin (*ply511*) with inherent broad lytic activity was introduced. Second, the lysogeny control region (LCR), which mediates prophage integration and maintenance, was deleted (Kilcher et al., 2018). We have previously shown that this virulent PSA derivative reduces the survival and clonal expansion of resistant cells, thus greatly improving its antibacterial efficacy (Kilcher et al., 2018).

Next, we partitioned the 36.1-kb genome of PSA ΔLCR *ply511* into six overlapping DNA fragments that were used to assemble full-length, synthetic, circular PSA genomes using the Gibson method (see Figures S1A and S1B). Critically, the fragment encoding only the PSA RBP (RBP fragment; 1,358 bp) was amplified using error-prone PCR (epPCR) to introduce targeted mutagenesis within this gene. To increase the fraction of viable phage genomes and to make sure that host-range mutants are

Figure 1. Gp15 Is the PSA Receptor Binding Protein and Binds Galactosylated Type II Wall Teichoic Acid

(A) Schematic representation of the WTA ribitol phosphate modifications of all used serovars.

(B) Transmission electron micrograph of a PSA virion. The baseplate is indicated with a black arrow.

(C) Schematic representation of the genomic region encoding the PSA baseplate and comparison to lactococcal phages TP901-1 and p2. Sequence and structure homologies are indicated with gray and pink shading, respectively.

(D) SDS-PAGE of purified full-length (FL) PSA GFP-gp15 (71.6 kDa) and of the GFP-gp15 C-terminal domain (CTD) (48.8 kDa).

(E and F) The ability of these proteins to bind *Listeria* cells with known WTA structure and glycosylation patterns was visualized by confocal microscopy (E) and quantified by fluorescence spectroscopy (F).

(G and H) To correlate RBP binding data with the phenotype of intact PSA virions, phage binding (G) and infection (H) assays were performed on the SV 4b strain WSLC1042 and on the indicated WSLC1042-derived WTA glycosylation mutants.

Fluorescence spectroscopy, phage binding, and phage infection data are mean ± SD (n = 3). ns = not significant; ** = p value < 0.01; *** = p value < 0.001; **** = p value < 0.0001. tmp, tape measure protein; gal, galactose; Glc, glucose; Rha, rhamnose; GlcNAc, N-acetylglucosamine; Ac, acetylation, hol, holin; ply, phage endolysin; C2/C4, C2 and C4 position of the WTA RboP backbone.

See also Table S1.

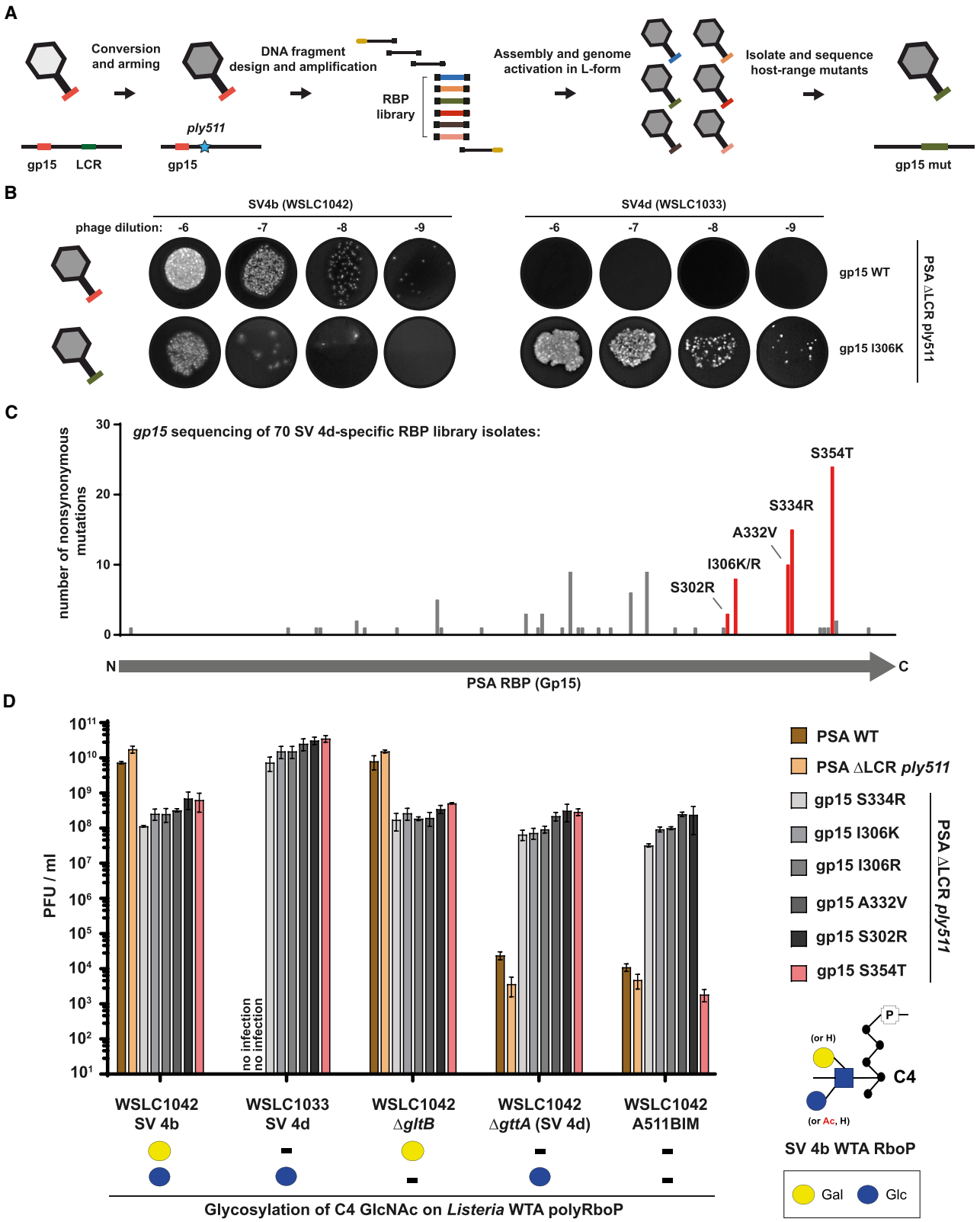

(legend on next page)

solely due to alterations in the RBP gene sequence, all non-RBP fragments required for synthetic genome assembly were produced with a high-fidelity polymerase. For the RBP fragment, DNA from three *gp15* epPCR reactions with low (1 mut/kb), medium (3.5 mut/kb), and high (5.8 mut/kb) mutagenesis rates were pooled and a synthetic genome library assembled *in vitro*. To obtain the corresponding phage library, the assembled genomic DNAs (gDNAs) were transfected into cell wall-deficient Rev2L L-form *Listeria* (Kilcher et al., 2018). Progeny phage are produced within L-forms and subsequently assayed for plaque formation on *Listeria* strains of diverse WTA composition (SVs 1/2, 4a, 4b, 4c, 4d, and 5) (Shen et al., 2017), which selects for viable phage mutants with altered host specificities. Naturally, many mutated gp15 sequences will be deleterious and therefore would not produce viable phages. Apart from the PSA host strain WSLC1042 (SV 4b), we identified plaques on the SV 4d strain WSLC1033, which lacks WTA galactosylation (see Figure 1A). A representative example of one host-range mutant (*gp15* I306K) is shown in Figure 2B. RBP sequencing of 70 SV 4d-infecting phage clones revealed that most underlying mutations were found in the Gp15 C terminus (Figure 2C). Six mutant phage isolates encoded only a single point mutation (S302R, I306K/R, A332V, S334R, and S354T), each of which was sufficient for a shift in host range from SV 4b to 4d and did not form plaques on any other *Listeria* SVs (Figure S1C).

To identify the receptor of these mutated RBPs, we quantified plating efficiencies on WSLC1042 (SV 4b), WSLC1033 (SV 4d), and on isogenic WSLC1042 WTA glycosylation mutants (Figure 2D). All six of the phages carrying a single RBP point mutation gained the ability to infect SV 4d strain WSLC1033 with high efficiency and infected WSLC1042 Δ*gttA*, which features SV 4d-like WTA glycosylation. This novel specificity came at the cost of 100-fold reduced plating efficiency on the original host. Thus, these phages possess a shifted rather than extended host range. Interestingly, five of the six mutants featured a relatively relaxed specificity toward RboP C4-GlcNAc. They infected all isogenic WTA mutants with equal efficiency, regardless of whether GlcNAc was non-glycosylated (WSLC1042_A511BIM), carried galactose (WSLC1042 Δ*gltB*), glucose (WSLC1042 Δ*gttA*), or both (WSLC1042) (Figure 2D). One PSA RBP mutant (*gp15* S354T) did not efficiently infect non-glycosylated GlcNAc but lost its galactose dependency. Overall, SV 4b and SV 4d WTAs are closely related and both feature glucosylated RboP C4-GlcNAc. Potentially, the generation of host-range mutants capable of binding and infecting more distantly related WTA compositions (e.g., C2-GlcNAc or type I WTAs) requires more extensive modification within the $Gp15_{CTD}$, which may not be achievable using epPCR.

A Chimeric PSA Incorporating Two Different RBPs Features an Extended Host Range

Analysis of *gp15* mutants revealed that the ability to infect strains with galactose-deficient WTA comes at the cost of reduced infection efficiency of the original host. To bypass this trade-off, we aimed at constructing a polyvalent phage, i.e., a phage that recognizes multiple receptor epitopes by engaging more than one RBP (de Jonge et al., 2019). To this end, we constructed a synthetic phage that encodes two adjacent RBP copies. The first copy is wild-type *gp15*, which mediates binding to galactosylated WTA whereas the second copy encoded a codon-optimized (CO) *gp15* featuring the S334R mutation ($gp15_{CO}$ S334R), whose product binds to unglycosylated or monoglycosylated WTA (Figure 3A). Because PSA contains multiple RBPs in one particle, we assumed this genotype would result in a phage with a chimeric baseplate composed of both Gp15 wild-type (WT) and Gp15 S334R proteins. For comparison, the TP901-1 baseplate incorporates 54 RBP proteins (18 homotrimers) (Veesler et al., 2012). As a control, to make sure that codon-optimization does not affect activity of the mutant phage carrying the *gp15* S334R gene, we replaced the gp15 S334R gene with $gp15_{CO}$ S334R, and show that this does not result in any phenotypic changes (Figure 3B, light- and dark-green bars): Again, we observed that *gp15* WT phage was restricted to galactosylated WTA, whereas both the non-codon-optimized and codon-optimized S334R mutants shared the same relaxed C4-GlcNAc specificity (Figure 3B). As before, this came at the cost of reduced infection efficiency of strains with galactosylated WTA. Finally, the polyvalent phage with two RBPs produced true chimeric particles that infect the SV 4b strain WSLC1042 with the same efficiency as the WT phage and feature a relaxed specificity toward the isogenic WSLC1042-derivatives that lack GlcNAc glycosylation (Figure 3B, blue bars). Interestingly, the polyvalent phage also infected the SV 4d strain WSLC1033 with decent efficiency but could not fully rescue infection compared to the original mutant (gp15 S334R). This may be a reflection of the complete inability of the WT Gp15 protein to mediate infection of this strain. In sum, based on a monovalent phage, this approach enabled the production of a polyvalent phage with an extended host range infecting *Listeria* SVs 4b and 4d as well as monoglycosylated and unglycosylated WTA mutants.

Crystal Structure of the Gp15 Carboxyl Terminus Reveals a Conserved RBP Domain Architecture

To better understand the molecular details of host adsorption by *Listeria*-targeting phages, as well as to map the identified *gp15* mutations that mediate host-range shift, we determined the

Figure 2. Isolation of Host-Range Shift Mutants by Diversification of RBP Sequences

(A) Workflow for the generation of phage libraries with diversified RBP sequence. To achieve random mutagenesis, the RBP DNA fragments were amplified using epPCR.

(B) Representative image of relative plating efficiencies of an isolated PSA mutant (*gp15* I306K) with preferential infection of a SV 4d strain WSLC1033.

(C) 70 SV 4d-specific PSA mutants were isolated and their RBP genes sequenced. The histogram represents the cumulative mutation frequencies of individual RBP amino acids. Red bars indicate the presence of PSA mutants that feature only one point mutation within the whole RBP.

(D) Efficiencies of plating of isolated *gp15* point mutants on SV 4b (WSLC1042) and SV 4d strains (WSLC1033), as well as on isogenic WSLC1042-derived WTA glycosylation mutants. WTA glycosylation patterns are indicated.

Data are mean ± SD (n = 3).

See also Figure S1.

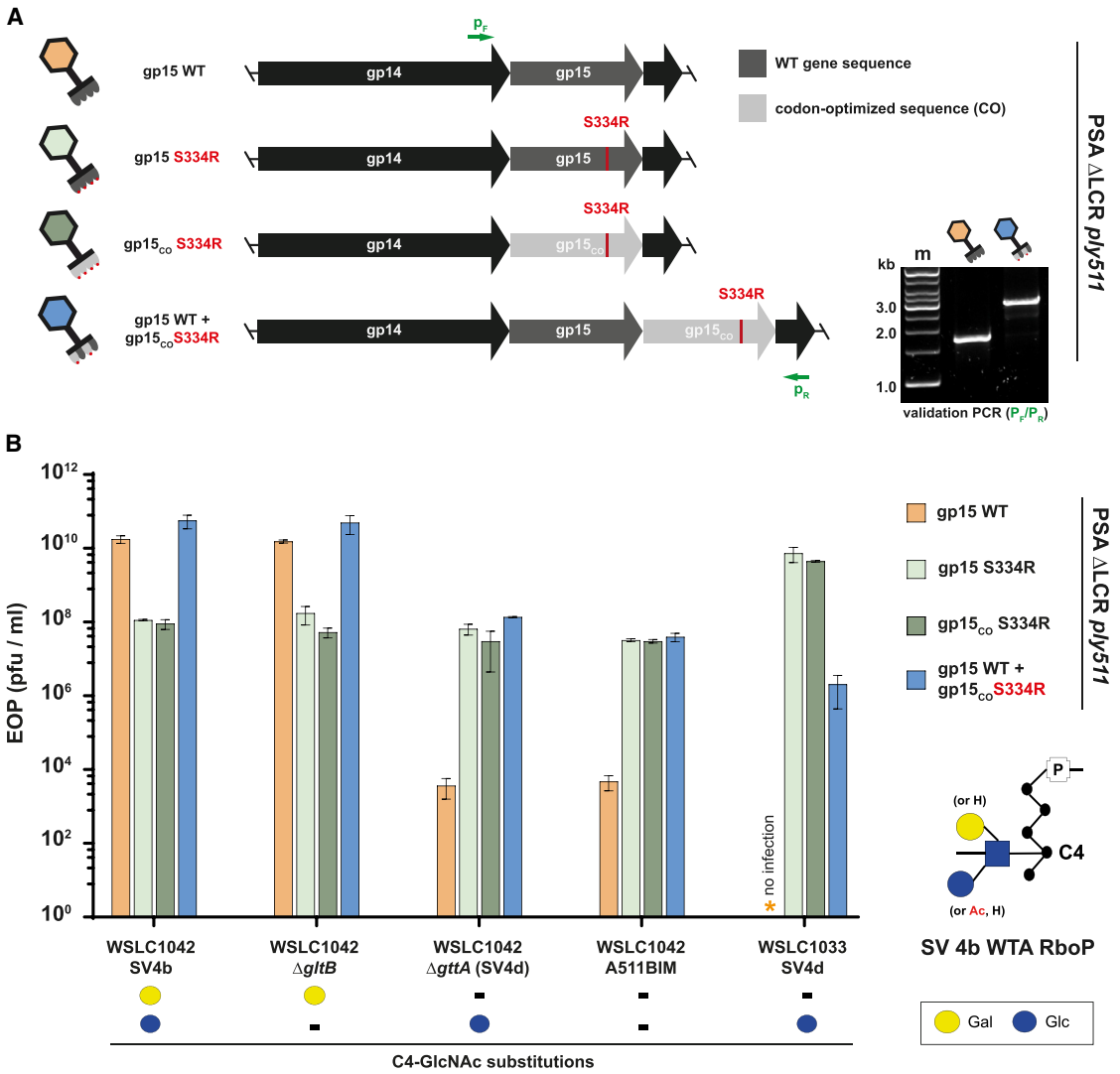

Figure 3. Construction of an Extended Host-Range Phage That Incorporates Two RBP Variants in a Single Baseplate

(A and B) Synthetic phages that encode the WT and/or the mutant (*gp15* S334R) RBPs were constructed as depicted in (A) and their plating efficiencies quantified on SV 4b cells (WSLC1042), SV 4d cells (WSLC1033), and on isogenic WSLC1042-derived WTA glycosylation mutants (B).

CO, codon optimized; P_F/P_R, primers used to validate genotype (see insert). Phage capsid and histogram bar colors correspond. Data are mean ± SD from three independent experiments.

crystal structure of the receptor-binding carboxyl terminus of PSA Gp15 to 1.7-Å resolution (Figure 4). The structure consists of a ~124-Å-long $Gp15_{CTD}$ homotrimer, which based on architectural similarities to well-studied lactococcal phage RBPs, can be split into three distinct domains: the N-terminal "stem" (Ala203–Ala232), central "neck" (Lys233–Ser259), and distal "head" (Val260–Thr373), with the latter mediating receptor binding (see Figures 4A and 5). Although absent from the $Gp15_{CTD}$ structure, bioinformatic analyses predicted the Gp15 N terminus (Leu4–Thr181) has structural similarity to the upper baseplate protein (BppU; ORF48) of phage TP901-1 (Veesler et al., 2012), which we propose is used to connect Gp15 to the phage baseplate. Together, the stem and neck domains form a segmented ~80-Å-long right-handed coiled coil. The stem features two helical bundles, HB1 and HB2, composed of 8 and 6 residues, respectively, and the neck domain forms a continuous 25-residue coiled coil that connects to the C-terminal head domain (Figures 4A and S2). Connecting these coils are triangular β layers (Hartmann, 2017) perpendicular to the axis of the trimer that invoke 120° rotations of the three helical chains around the central axis to provide a simple and compact transition between the helical bundles and the coiled coil of the neck domain. Distal to the neck is the head domain, which consists of nine β sheets folded into a quasi-double Greek key fold (Figure S3) that closely resembles the head domains of other lactococcal (Ricagno et al., 2006; Spinelli et al., 2006a, 2006b) and mammalian virus (Reiss et al., 2012; Singh et al., 2018) RBPs (Figure 5). It remains to be studied how topological changes made by the error-prone

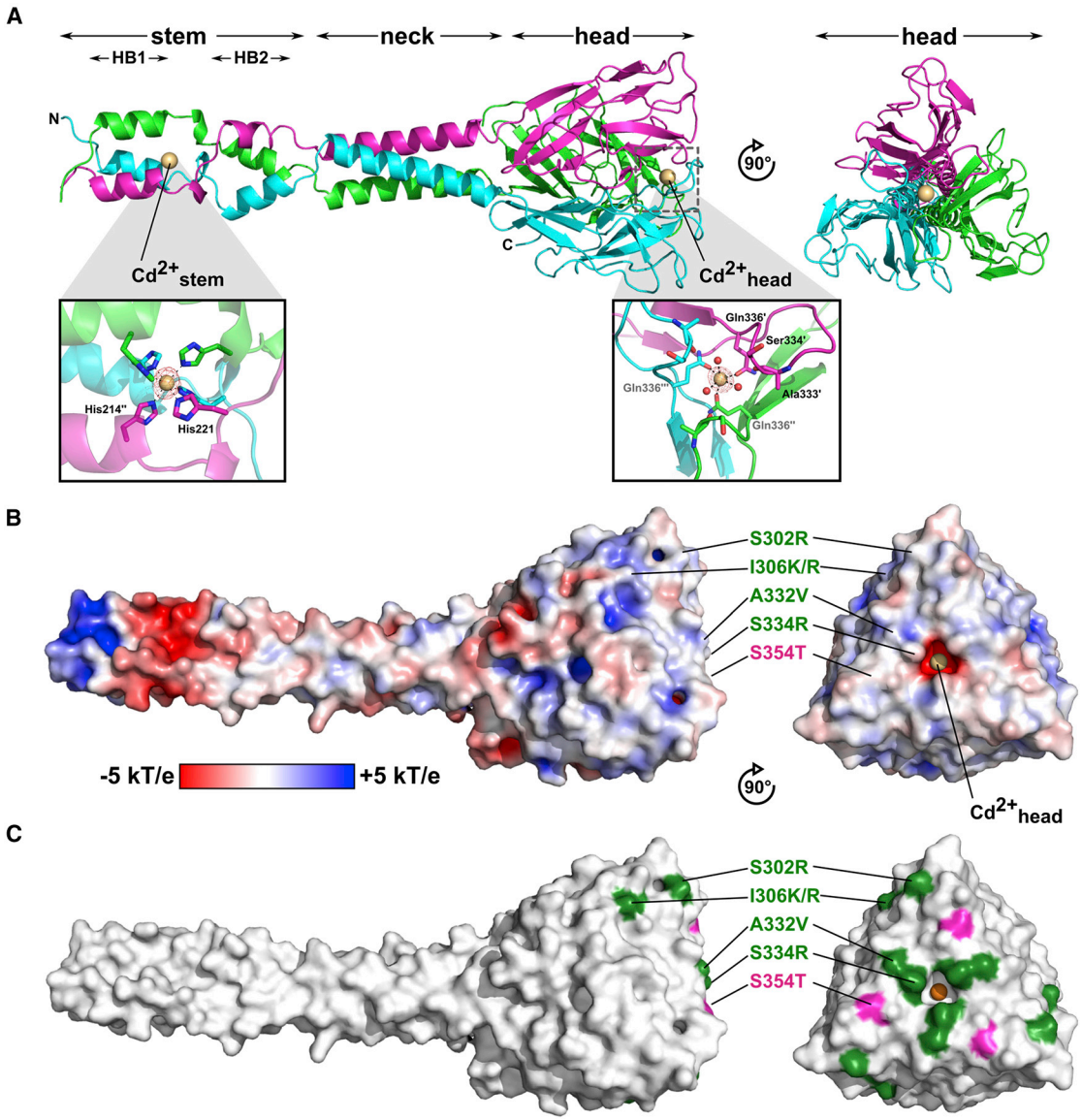

Figure 4. Crystal Structure of the Receptor-Binding Carboxyl Terminus of the PSA Tail Spike

(A) Ribbon diagram of the $Gp15_{CTD}$ homotrimeric complex with individual chains colored magenta, cyan, and green. Highlighted are the stem, neck, and head domains, including helical bundle subdomains (HB1 and HB2) of the stem. Represented as brown spheres, and highlighted as cutaway panels, are two coordinated cadmium ions: Cd^{2+}_{stem} within the interface between HB1 and the connecting β layer, and Cd^{2+}_{head} within a negatively charged cavity at the center of the RBP 3-fold axis on the bottom of the head domains. Red mesh is the anomalous Fourier difference map contoured at 5.0σ. For both ions, interacting residues (shown as sticks) and water molecules (red spheres) all form near-perfect octahedral coordination. Black dashed lines indicate coordination bonds of Cd^{2+}_{stem} with side-chain Nε2 group of His214 and 221 (bond lengths of 2.45–2.61 Å), and Cd^{2+}_{head} with side-chain Oε group of Gln336 and three water molecules (bond lengths of 2.37–2.59 Å).

(B) Molecular surface of the RBP complex colored according to its electrostatic surface potential (±5 kT/e) generated by Adaptive Poisson-Boltzmann Solver (APBS). Highlighted are the five residues and their mutations produced by error-prone PCR that caused PSA phage host-range adaptation.

(C) Molecular surface of the PSA RBP colored white with above-mentioned host-range mutants colored green to identify those that are adapted to recognize non-glycosylated C4 GlcNAc, and colored magenta, the S354T mutant that loses galactose binding specificity.

See also Figure S2 and Table S7.

mutants affect receptor interactions. However, all verified mutants mapped to protruding loops at the distal end of the Gp15 head domain, where WTA binding most likely occurs (Figures 4B and 4C). None of these side chains directly contributes to pocket formation, where typical ligand binding is expected to occur. Instead, mutations S302R, I306K/R, and S334R introduce positive surface charge, which could potentially increase electrostatic interactions with the RboP WTA backbone. The S334R mutation introduces positive charge around a large, divalent cation-binding cavity (Cd^{2+}_{head}) on the base of the head

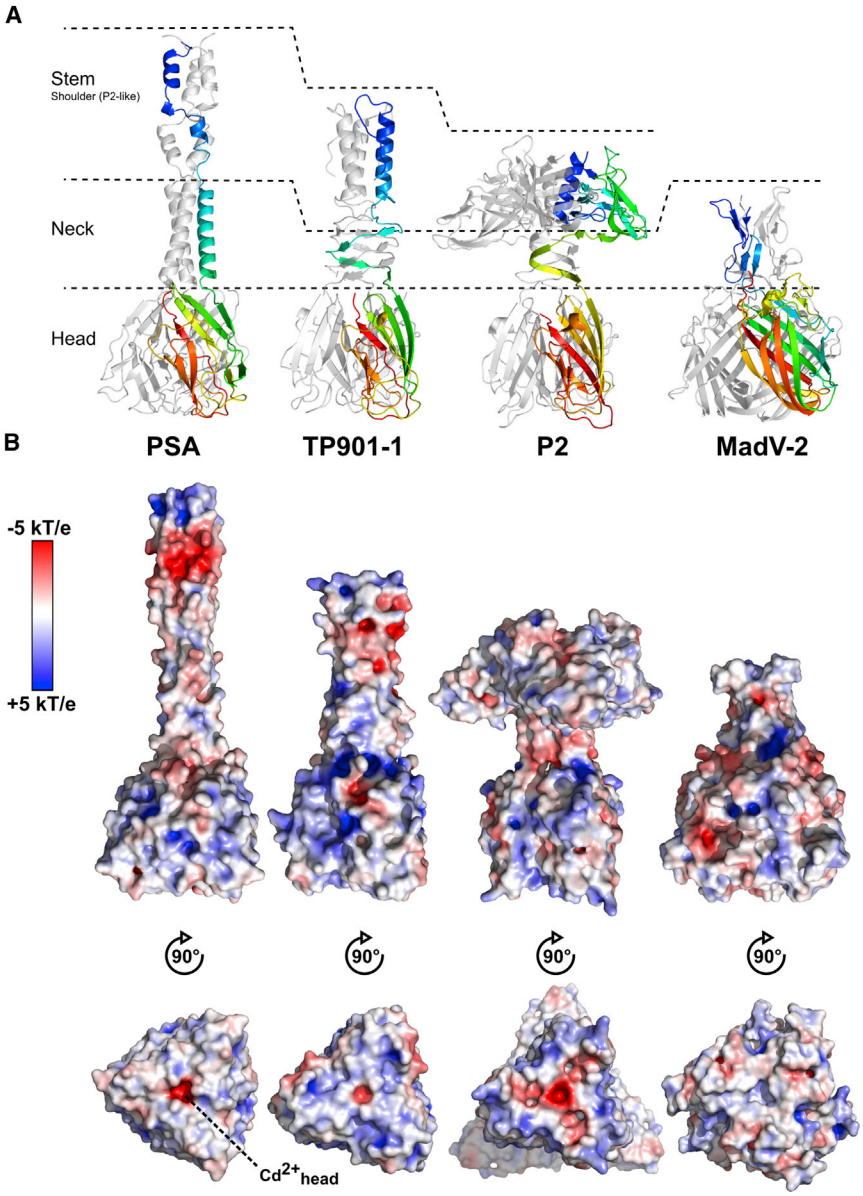

Figure 5. Structural Homology of Viral RBPs

(A) Shown as ribbon diagrams and aligned horizontally are homotrimeric RBPs from phage PSA (Gp15) and lactococcal phages TP901-1 (Gp49; PDB: 3EJC; Bebeacua et al., 2010) and P2 (Gp18; PDB: 2BSD; Spinelli et al., 2006b), and the homotrimeric tip of the murine adenovirus 2 (MadV-2) fiber (PDB: 5NC1; Singh et al., 2018). Boundaries of the stem (or shoulder domain for P2), neck, and head domains are shown as dashed lines.

(B) Molecular surface of each complex is colored according to its electrostatic surface potential (±5 kT/e) generated by APBS. The base of all three phage RBP head domains features a negatively charged pocket, central to the RBP 3-fold axis. Only PSA features metal binding within this pocket (Cd^{2+}_{head}) (Figure 4). CASTp 3.0 (Tian et al., 2018) analysis revealed a solvent-accessible volume of 23.1 $Å^3$ (surface area, 69.3 $Å^2$) for this pocket formed by Ala333, Ser334, and Gln336 residues of all three Gp15 chains. For comparison, CASTp 3.0 calculated the corresponding pocket of P2 with an internal volume of only 1.17 $Å^3$ (surface area, 5.75 $Å^2$), and no pocket was identified for TP901-1; thus, despite similarities in surface potential, it is not likely that Cd^{2+}_{head}-like metal binding occurs on the base of these lactococcal RBP heads. See also Figure S3.

domain (Figure 5B). However, as the S334 side chain is not directly involved in metal coordination, it remains unclear whether this mutation affects ion binding. The other two mutants, A332V and S354T, do not alter hydrophobicity or polarity, respectively, but feature slightly larger side chains. It remains to be determined how such subtle differences in surface properties mediate binding to galactose-deficient WTA.

Redirecting Phage Specificity through Structure-Guided Engineering of Chimeric Phages with Prophage-Derived RBP Domains

RBP sequence randomization enabled binding of strains with closely related WTAs (Figure 2). To target structurally more divergent WTAs, we resorted to bioinformatics analysis of putative, prophage-encoded RBPs in sequenced *Listeria* genomes. We hypothesized that PSA-like prophages encoded within published *Listeria* strains should be able to bind the WTAs of their lysogenized host, i.e., carry SV-specific RBPs. 20 PSA-like RBP candidates were identified within SVs 1/2 (12 lysogens), 4a (1 lysogen), 4b (5 lysogens), 5 (1 lysogen), and 6b (1 lysogen) strains (Figure 6A; Table S2). Multiple sequence alignment revealed limited sequence homology within the N-terminal BppU-like and C-terminal head domains (Figure 6A); however, high sequence conservation was observed within the central stem and neck, especially within the connecting β-layer regions (Figures 6C and S2). The stem and neck most likely form conserved connectors for multiple phage baseplate types and specificity domains. For instance, His_{214} and His_{221} that form the metal binding site of HB1 (Cd^{2+}_{Stem}) are 100% conserved in all 20 RBPs, implying conservation of metal coordination within stems of different *Listeria*-binding RBPs. Presumably, the repetitive nature of segmented coiled coils with short universal adapters such as β layers (see Figure S2) provides these phages with a simple, exploitable backbone to facilitate reshuffling of homologous modules by genetic recombination. For PSA and PSA-like RBPs, this would provide a potential mechanism to fine-tune host recognition in order to overcome ever-adapting host defenses.

To confirm our initial hypothesis, phylogenetic analysis revealed that the 20 identified head domains clustered

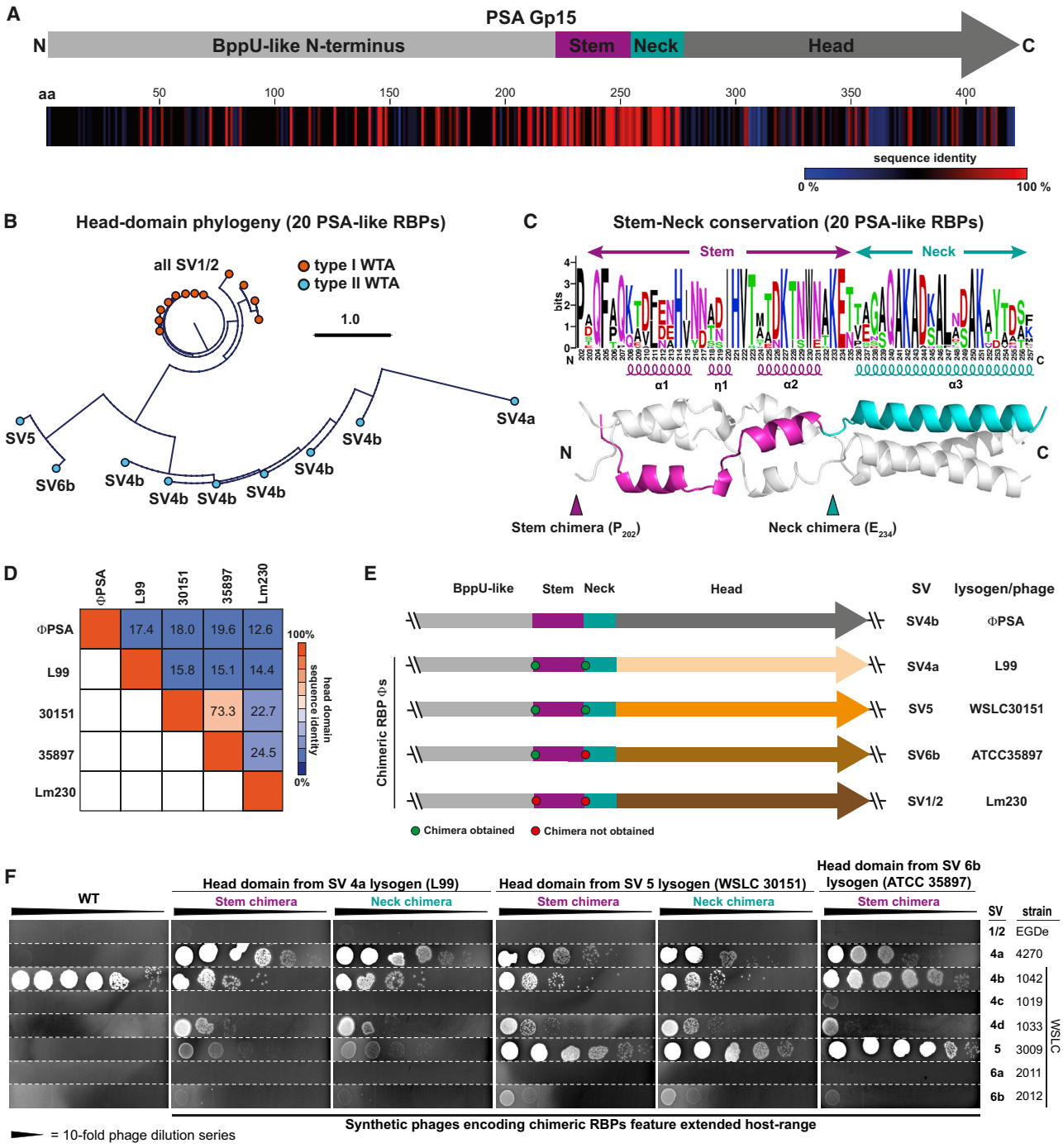

Figure 6. Structure- and Sequence-Guided Construction of Chimeric Phages with Modified Host Range

PSA-like RBPs were identified in published, SV-annotated *Listeria* genomes using the stem and neck domains as protein blast query sequences.

(A) Multiple sequence alignment of 20 *Listeria* prophage encoded RBP candidates suggests that the PSA stem-neck domains connect distinct head domains to distinct BppU-like N termini.

(B) A phylogenetic tree of the identified Gp15-like head domains reveals clustering according to SV/WTA type.

(C) Analysis of the stem-neck-domain consensus sequence and the corresponding crystal structure revealed highly conserved β sheets connecting the stem to the N-terminal BppU-like domain and the α3 coiled coil to the α2 HB2 of the stem region. Conserved residues within these two linker regions were selected as exchange sites for the construction of stem (P_{202}) and neck (E_{234}) chimeras, respectively.

(legend continued on next page)

according to the SV of the lysogen from which they were identified (Figure 6B). Furthermore, head domains of type I (SV 1/2) and type II (SVs 4a, 4b, 5, 6b) WTA-containing strains formed more distantly related clusters, reflecting the fundamental difference of their RboP connectivity.

In order to reprogram PSA host specificity, we attempted a structure- and sequence-guided design of engineered PSA derivatives with chimeric RBPs. To this end, we exchanged the head domain of Gp15 with prophage-encoded RBP head domains. This approach should maintain the structural integrity of the PSA baseplate, i.e., the interactions of the Gp15 N terminus with other baseplate proteins. Head domain substitutions were attempted at two locations within the stem-neck region that are (1) 100% conserved among the 20 candidates and (2) not located within secondary structure elements (Figure 6C). Based on these criteria, "stem chimeras" were fused after a conserved proline (Pro_{202}) upstream of HB1 (α1), whereas "neck chimeras" were fused after a conserved glutamic acid (Glu_{234}) upstream of the α3 coiled coil (see Figure 6C). Heterologous domains were selected from four lysogens, covering SVs 1/2, 4a, 5, and 6b (L99, 30151, 35897, and Lm230; see Table S2). It is worth noting that the corresponding head domains share only 13%–25% protein sequence identity with each other and with the PSA head domain (Figure 6D). Exceptions are the SV 5 and SV 6b lysogens (73.3% identity), which likely reflects their identical RboP glycosylation pattern (Shen et al., 2017) (see also Figure 1A). Using PSA ΔLCR *ply511* as a backbone, we constructed the chimeric phage genomes shown in Figure 6E (see also Table S4). We were able to isolate corresponding chimeric phages for all tested heterologous head domains, except for the predicted SV 1/2-binding domain derived from lysogen Lm230, which was able to bind SV 1/2 cells when expressed as a GFP-RBP_{CTD} fusion protein (see Figure S4A). Synthetic phages were isolated and sequenced, and plating efficiencies were determined on representative strains of all major *Listeria* SVs (Figures 6F and S4B). All chimeric phages featured an extended host range, with preferential infection of hosts whose WTA structures match the expected SV specificity of the heterologous head domain. Interestingly, the chimeras were significantly more broad range than PSA WT and were able to plaque on strains with poly-RboP chains connected via C2 and C4 GlcNAc, whereas PSA Gp15 was restricted to C4 GlcNAc. SVs 5 and 6b feature identical WTA structure. Consequently, chimeras with head domains from WSLC30151 (SV 5) and ATCC35897 (SV 6b) both infected SV 5 (Figure 6F). Plaque formation on SV 6b could not be observed, potentially due to intracellular defense mechanisms. In support of this notion, we were able to demonstrate binding of these SV 5/6b-specific chimeras to SV 6b strain WSLC2012 (Figure S4C). The stem chimera with the ATCC 35897 (SV 6b) head domain infected SV 4b and SV 5 with similar efficiency, suggesting that it can bind the broadest range of WTA structures. Finally, we created a phage cocktail containing all stem chimeras, the SV 4d-specific *gp15* point mutant (S334R), as well as the PSA WT phage. This PSA scaffold-based cocktail infected SVs 4a, 4b, 4d, and SV 5 with comparable efficiency (Figure S4D). Overall, we show that identification of functional RBPs through pathogen-specific RBP database search is an efficient approach for the design of chimeric phages with altered and predictable host ranges.

DISCUSSION

The ability to engineer RBP-host receptor interactions is an important prerequisite for the development of effective phage therapeutics against specific bacterial pathogens. A bottleneck in phage host-range engineering is the high structural diversity of cell surface receptors (Dunne et al., 2018b; Wang et al., 2010), which include lipopolysaccharide epitopes on the surface of Gram-negative pathogens bound by T7-like phages (Bertozzi Silva et al., 2016) or teichoic acids and pellicle polysaccharides bound by phages of Gram-positive bacteria (Dunne et al., 2018b). Despite the previous development of host-range engineering strategies for T7-like phages targeting Enterobacteriacea (Ando et al., 2015; Yosef et al., 2017; Yehl et al., 2019), similar approaches for Gram-positive targeting phages have not previously been achieved. Using our recently developed synthetic phage engineering platform (Kilcher et al., 2018) and *Listeria* as a model system, we present several approaches for rational engineering of phages targeting such Gram-positive pathogens. The first approach is based on RBP-directed mutagenesis and does not depend on prior knowledge of the RBP structure or its receptor epitope. This directed-evolution approach accelerates phage-host coevolution by artificially increasing the mutation rate in a gene-specific manner. As previously demonstrated for other RBPs (Le et al., 2013), we show that single amino acid substitutions are sufficient to change RBP specificity between closely related receptors, e.g., point mutations within PSA *gp15* (S302R, I306K/R, A332V, S334R, and S354T) that shift specificity from SV 4b to SV 4d (Figure 2). After identifying such host-range-altering mutations, our second approach involves the construction of a polyvalent phage that encodes both WT and mutated RBPs in a synthetic PSA phage genome (e.g., PSA ΔLCR *ply511 gp15*_WT $gp15_{CO}$_S334R infecting SVs 4b and 4d; see Figure 3). For our last approach, we solve the crystal structure of Gp15 to provide a blueprint for structure-guided design of phages with chimeric RBPs and altered host specificities. Chimeric RBPs were designed using PSA-compatible, heterologous binding domains that were extracted from sequenced *Listeria* strains that carry prophages. The host specificities of these heterologous head domains were predicted phylogenetically and by lysogen serotyping (Figure 6). As sequenced prophages greatly outnumber isolated and characterized lytic viruses, published genome sequences provide an extensive resource of RBP genes that can be used in the design and production of chimeric phages with altered tropism. Using this approach, we generated five synthetic

(D–F) Head domains with predicted SV 4a (from strain L99), SV 5 (30151), SV 6b (35897), and SV 1/2 (Lm230)-specificity share only very limited sequence identity (D) and were selected for the construction of stem- and neck-chimeric phages as shown in (E). Host ranges and infection efficiencies of these synthetic PSA ΔLCR ply511-derived phage chimeras were determined using spot-on-lawn assays on representative *Listeria* strains of the indicated SVs (F).
See also Figure S4 and Table S2.

phages featuring chimeric RBPs that extend the host range from SV 4b to SVs 4a, 4b, 4d, and 5 (Figure 6; Table 1). Interestingly, we were able to generate functional chimeras using prophage-encoded head domains with very low sequence similarity. For instance, the SV 4a-binding head domain derived from *Listeria* strain L99 (locus-tag: lmo4a_2606) enabled host range expansion, yet only shares 17.4% sequence identity with the PSA *gp15* head domain. This is in sharp contrast to the CTDs of T7-like tail fibers used previously for host range modulation, which typically share >80% sequence identity even between phages infecting different genera (Ando et al., 2015).

While switching specificity between type II WTA-based receptors was successful, it remains to be determined why functional, type I WTA-specific RBPs (see Figure S4A) did not produce viable PSA chimeras. Possibly, other PSA baseplate proteins such as Dit, Tal, or the BppU domain of Gp15 are involved in yet-unidentified phage-WTA interactions. Such interactions may be required for binding, cell wall penetration, or DNA injection but are not compatible with type I WTA architecture. To circumvent this limitation, the presented host range programming strategies could be applied to other *Listeria* siphoviruses that have the inherent ability to target both type I and type II WTAs, such as phages P70 or P40 (Klumpp and Loessner, 2013). Alternatively, a cocktail of one type I and one type II WTA-specific phage backbone may be enough to cover all SVs.

Over the last decade, the molecular mechanisms of host interaction by phages and their intricate baseplate complexes have been studied intensely using cryoelectron microscopy (cryo-EM) and X-ray crystallography (Bebeacua et al., 2010; Guerrero-Ferreira et al., 2019; Hu et al., 2015; Plisson et al., 2007; Sciara et al., 2010; Taylor et al., 2016; Veesler et al., 2012), providing high-resolution details for this fundamental stage of phage infection. Regarding *Listeria*-targeting phages, cryo-EM studies on the myovirus A511 baseplate revealed large structural transformations of this molecular machine, whereby *Listeria* cell binding of peripheral tail fibers triggers the release and reorientation of secondary RBPs toward the bacterial cell wall (Guerrero-Ferreira et al., 2019).

Here, we present the high-resolution crystal structure of the carboxyl terminus of the PSA RBP (Gp15). An interesting feature of Gp15 is the trimeric α-helical coiled coil that constitutes the neck domain, whereas all structurally related RBPs, i.e., *Lactococcal* phages p2 (Spinelli et al., 2006b), TP901-1 (Spinelli et al., 2006a), and Tuc2009 (Legrand et al., 2016) (and most likely bIL170; Ricagno et al., 2006), instead contain trimeric interlaced β-helical necks (Figure 5). Together, stem and neck domains function as linking units that connect the receptor binding domains to the rest of the baseplate. As such, the presence of conserved stem and neck domains within particular phage types is likely indicative of head domain compatibility, because these domains determine the tolerable size and relative positioning of the individual head domain monomers. This information is important for the identification of heterologous head domains that yield viable chimeric phages. In order to broaden the applicability of host range programming to phages with other baseplate architectures, it will thus be important to determine additional RBP structures. This will lead to the identification of other RBP types and linking domains that are conserved in multiple phage genomes. Interestingly, protein-protein BLAST (BLASTp) analysis of the PSA stem and neck reveals conservation of these domains in *Bacillus* genomes (Table S5), suggesting these connectors are conserved across genus boundaries. Similar observations have previously been made for *S. aureus* φ11, whose overall RBP architecture is found in many phages that target Gram-negative bacteria (Dunne et al., 2018b). This suggest that host-range engineering across genus boundaries may be possible; however, this will require additional engineering steps to provide compatible tail-associated lysins, promoters, and lysis cassettes, to mention just a few potential obstacles.

While much still needs to be learned about the molecular details of RBP-receptor interactions, we envision that the approaches presented in this study will allow for the design of customized phage antimicrobials and phage-based DNA delivery vectors that are based on a limited number of well-characterized scaffolds, whose host specificities can be programmed according to the requirements of each application. Such customized vectors will simplify regulatory approval of novel phage biologics, generate additional opportunities to obtain intellectual property, and boost the development of phage-based precision medicines.

STAR★METHODS

Detailed methods are provided in the online version of this paper and include the following:

- KEY RESOURCES TABLE
- LEAD CONTACT AND MATERIALS AVAILABILITY
- EXPERIMENTAL MODEL AND SUBJECT DETAILS
  - Bacterial strains and bacteriophages
- METHOD DETAILS
  - Protein expression and purification
  - Cell wall decoration assay
  - Phage binding assay
  - Protein crystallization
  - Data collection and refinement
  - Transmission Electron Microscopy of PSA phage particles
  - Phage genome assembly and activation by transfection into Listeria L-forms
  - RBP diversification
  - Identification of prophage-encoded Gp15-like RBPs
  - Bioinformatics
- QUANTIFICATION AND STATISTICAL ANALYSIS
- DATA AND CODE AVAILABILITY

SUPPLEMENTAL INFORMATION

Supplemental Information can be found online at https://doi.org/10.1016/j.celrep.2019.09.062.

ACKNOWLEDGMENTS

S.K. was supported by the Swiss National Science Foundation (PZ00P3_174108). We are grateful to Peer Mittl from the Department of Biochemistry, University of Zurich, for helpful discussions and advice regarding crystal structure refinement. We would also like to thank Beat

Blattmann from the Protein Crystallization Center (PCC) at University of Zurich, and the staff from the Scientific Center for Optical and Electron Microscopy (ScopeM), ETH Zurich, and beamline X06SA of the Swiss Light Source (Paul Scherrer Institute, Villigen).

AUTHOR CONTRIBUTIONS

Conceptualization, M.D. and S.K.; Funding Acquisition, S.K. and M.J.L.; Investigation, M.D., B.R., M.T., X.Q., P.E., L.H., and S.K.; Project Administration, S.K.; Resources, S.K., A.P., and M.J.L.; Supervision, M.D., A.P., M.J.L., and S.K.; Validation, M.D. and S.K.; Visualization, M.D., Y.S., and S.K.; Writing – Original Draft, M.D. and S.K.; Writing – Review and Editing, M.D., Y.S., E.S., M.J.L., and S.K.

DECLARATION OF INTERESTS

The authors declare no competing interests.

Received: April 23, 2019
Revised: August 7, 2019
Accepted: September 19, 2019
Published: October 29, 2019

REFERENCES

Adams, P.D., Afonine, P.V., Bunkóczi, G., Chen, V.B., Davis, I.W., Echols, N., Headd, J.J., Hung, L.W., Kapral, G.J., Grosse-Kunstleve, R.W., et al. (2010). PHENIX: a comprehensive Python-based system for macromolecular structure solution. Acta Crystallogr. D Biol. Crystallogr. *66*, 213–221.

Altschul, S.F., Gish, W., Miller, W., Myers, E.W., and Lipman, D.J. (1990). Basic local alignment search tool. J. Mol. Biol. *215*, 403–410.

Ando, H., Lemire, S., Pires, D.P., and Lu, T.K. (2015). Engineering modular viral scaffolds for targeted bacterial population editing. Cell Syst. *1*, 187–196.

Baker, N.A., Sept, D., Joseph, S., Holst, M.J., and McCammon, J.A. (2001). Electrostatics of nanosystems: application to microtubules and the ribosome. Proc. Natl. Acad. Sci. USA *98*, 10037–10041.

Bebeacua, C., Bron, P., Lai, L., Vegge, C.S., Brøndsted, L., Spinelli, S., Campanacci, V., Veesler, D., van Heel, M., and Cambillau, C. (2010). Structure and molecular assignment of lactococcal phage TP901-1 baseplate. J. Biol. Chem. *285*, 39079–39086.

Bertozzi Silva, J., Storms, Z., and Sauvageau, D. (2016). Host receptors for bacteriophage adsorption. FEMS Microbiol. Lett. *363*, fnw002.

Bikard, D., Euler, C.W., Jiang, W., Nussenzweig, P.M., Goldberg, G.W., Duportet, X., Fischetti, V.A., and Marraffini, L.A. (2014). Exploiting CRISPR-Cas nucleases to produce sequence-specific antimicrobials. Nat. Biotechnol. *32*, 1146–1150.

Cambillau, C. (2015). Bacteriophage module reshuffling results in adaptive host range as exemplified by the baseplate model of listerial phage A118. Virology *484*, 86–92.

Chen, V.B., Arendall, W.B., 3rd, Headd, J.J., Keedy, D.A., Immormino, R.M., Kapral, G.J., Murray, L.W., Richardson, J.S., and Richardson, D.C. (2010). MolProbity: all-atom structure validation for macromolecular crystallography. Acta Crystallogr. D Biol. Crystallogr. *66*, 12–21.

Chen, M., Zhang, L., Abdelgader, S.A., Yu, L., Xu, J., Yao, H., Lu, C., and Zhang, W. (2017). Alterations in gp37 expand the host range of a T4-like phage. Appl. Environ. Microbiol. *83*, e01576-17.

Citorik, R.J., Mimee, M., and Lu, T.K. (2014). Sequence-specific antimicrobials using efficiently delivered RNA-guided nucleases. Nat. Biotechnol. *32*, 1141–1145.

de Jonge, P.A., Nobrega, F.L., Brouns, S.J.J., and Dutilh, B.E. (2019). Molecular and evolutionary determinants of bacteriophage host range. Trends Microbiol. *27*, 51–63.

Dunne, M., Denyes, J.M., Arndt, H., Loessner, M.J., Leiman, P.G., and Klumpp, J. (2018a). *Salmonella* phage S16 tail fiber adhesin features a rare polyglycine rich domain for host recognition. Structure *26*, 1573–1582.e4.

Dunne, M., Hupfeld, M., Klumpp, J., and Loessner, M.J. (2018b). Molecular basis of bacterial host interactions by Gram-positive targeting bacteriophages. Viruses *10*, 397.

Duplessis, M., and Moineau, S. (2001). Identification of a genetic determinant responsible for host specificity in *Streptococcus thermophilus* bacteriophages. Mol. Microbiol. *41*, 325–336.

Dupuis, M.E., and Moineau, S. (2010). Genome organization and characterization of the virulent lactococcal phage 1358 and its similarities to *Listeria* phages. Appl. Environ. Microbiol. *76*, 1623–1632.

Edgar, R., Friedman, N., Molshanski-Mor, S., and Qimron, U. (2012). Reversing bacterial resistance to antibiotics by phage-mediated delivery of dominant sensitive genes. Appl. Environ. Microbiol. *78*, 744–751.

Emsley, P., Lohkamp, B., Scott, W.G., and Cowtan, K. (2010). Features and development of Coot. Acta Crystallogr. D Biol. Crystallogr. *66*, 486–501.

Eugster, M.R., Morax, L.S., Hüls, V.J., Huwiler, S.G., Leclercq, A., Lecuit, M., and Loessner, M.J. (2015). Bacteriophage predation promotes serovar diversification in *Listeria monocytogenes*. Mol. Microbiol. *97*, 33–46.

Gordillo Altamirano, F.L., and Barr, J.J. (2019). Phage therapy in the postantibiotic era. Clin. Microbiol. Rev. *32*, e00066-18.

Goren, M., Yosef, I., and Qimron, U. (2017). Sensitizing pathogens to antibiotics using the CRISPR-Cas system. Drug Resist. Updat. *30*, 1–6.

Guerrero-Ferreira, R.C., Hupfeld, M., Nazarov, S., Taylor, N.M., Shneider, M.M., Obbineni, J.M., Loessner, M.J., Ishikawa, T., Klumpp, J., and Leiman, P.G. (2019). Structure and transformation of bacteriophage A511 baseplate and tail upon infection of *Listeria* cells. EMBO J. *38*, e99455.

Habann, M., Leiman, P.G., Vandersteegen, K., Van den Bossche, A., Lavigne, R., Shneider, M.M., Bielmann, R., Eugster, M.R., Loessner, M.J., and Klumpp, J. (2014). Listeria phage A511, a model for the contractile tail machineries of SPO1-related bacteriophages. Mol. Microbiol. *92*, 84–99.

Hartmann, M.D. (2017). Functional and structural roles of coiled coils. Subcell. Biochem. *82*, 63–93.

Holm, L., and Rosenström, P. (2010). Dali server: conservation mapping in 3D. Nucleic Acids Res. *38*, W545–W549.

Hu, B., Margolin, W., Molineux, I.J., and Liu, J. (2015). Structural remodeling of bacteriophage T4 and host membranes during infection initiation. Proc. Natl. Acad. Sci. USA *112*, E4919–E4928.

Hupfeld, M., Fouts, D.E., Loessner, M.J., and Klumpp, J. (2015). Genome Sequences of the *Listeria ivanovii* subsp. *ivanovii* type strain and two *Listeria ivanovii* subsp. *londoniensis* strains. Genome Announc. *3*, e01440-14.

Joosten, R.P., Long, F., Murshudov, G.N., and Perrakis, A. (2014). The PDB_REDO server for macromolecular structure model optimization. IUCrJ *1*, 213–220.

Kabsch, W. (2010). Xds. Acta Crystallogr. D Biol. Crystallogr. *66*, 125–132.

Kamisango, K., Fujii, H., Okumura, H., Saiki, I., Araki, Y., Yamamura, Y., and Azuma, I. (1983). Structural and immunochemical studies of teichoic acid of *Listeria monocytogenes*. J. Biochem. *93*, 1401–1409.

Kilcher, S., and Loessner, M.J. (2019). Engineering bacteriophages as versatile biologics. Trends Microbiol. *27*, 355–367.

Kilcher, S., Loessner, M.J., and Klumpp, J. (2010). *Brochothrix thermosphacta* bacteriophages feature heterogeneous and highly mosaic genomes and utilize unique prophage insertion sites. J. Bacteriol. *192*, 5441–5453.

Kilcher, S., Studer, P., Muessner, C., Klumpp, J., and Loessner, M.J. (2018). Cross-genus rebooting of custom-made, synthetic bacteriophage genomes in L-form bacteria. Proc. Natl. Acad. Sci. USA *115*, 567–572.

Klumpp, J., and Loessner, M.J. (2013). *Listeria* phages: genomes, evolution, and application. Bacteriophage *3*, e26861.

Kot, W., Hammer, K., Neve, H., and Vogensen, F.K. (2013). Identification of the receptor-binding protein in lytic *Leuconostoc pseudomesenteroides* bacteriophages. Appl. Environ. Microbiol. *79*, 3311–3314.

Krissinel, E., and Henrick, K. (2007). Inference of macromolecular assemblies from crystalline state. J. Mol. Biol. *372*, 774–797.

Le, S., He, X., Tan, Y., Huang, G., Zhang, L., Lux, R., Shi, W., and Hu, F. (2013). Mapping the tail fiber as the receptor binding protein responsible for differential host specificity of *Pseudomonas aeruginosa* bacteriophages PaP1 and JG004. PLoS ONE *8*, e68562.

Legrand, P., Collins, B., Blangy, S., Murphy, J., Spinelli, S., Gutierrez, C., Richet, N., Kellenberger, C., Desmyter, A., Mahony, J., et al. (2016). The atomic structure of the phage tuc2009 baseplate tripod suggests that host recognition involves two different carbohydrate binding modules. MBio *7*, e01781-15.

Loessner, M.J., Estela, L.A., Zink, R., and Scherer, S. (1994). Taxonomical classification of 20 newly isolated *Listeria* bacteriophages by electron microscopy and protein analysis. Intervirology *37*, 31–35.

Loessner, M.J., Kramer, K., Ebel, F., and Scherer, S. (2002). C-terminal domains of *Listeria monocytogenes* bacteriophage murein hydrolases determine specific recognition and high-affinity binding to bacterial cell wall carbohydrates. Mol. Microbiol. *44*, 335–349.

Mahichi, F., Synnott, A.J., Yamamichi, K., Osada, T., and Tanji, Y. (2009). Site-specific recombination of T2 phage using IP008 long tail fiber genes provides a targeted method for expanding host range while retaining lytic activity. FEMS Microbiol. Lett. *295*, 211–217.

Marti, R., Zurfluh, K., Hagens, S., Pianezzi, J., Klumpp, J., and Loessner, M.J. (2013). Long tail fibres of the novel broad-host-range T-even bacteriophage S16 specifically recognize *Salmonella* OmpC. Mol. Microbiol. *87*, 818–834.

McCarville, J.L., Caminero, A., and Verdu, E.F. (2016). Novel perspectives on therapeutic modulation of the gut microbiota. Therap. Adv. Gastroenterol. *9*, 580–593.

Molineux, I.J. (2006). The T7 group. In The Bacteriophages, R. Calendar, ed. (Oxford University Press), pp. 277–301.

Nilsson, A.S. (2014). Phage therapy—constraints and possibilities. Ups. J. Med. Sci. *119*, 192–198.

Pape, T., and Schneider, T.R. (2004). HKL2MAP: a graphical user interface for macromolecular phasing with SHELX programs. J. Appl. Cryst. *37*, 843–844.

Philipson, C.W., Voegtly, L.J., Lueder, M.R., Long, K.A., Rice, G.K., Frey, K.G., Biswas, B., Cer, R.Z., Hamilton, T., and Bishop-Lilly, K.A. (2018). Characterizing phage genomes for therapeutic applications. Viruses *10*, 188.

Plisson, C., White, H.E., Auzat, I., Zafarani, A., São-José, C., Lhuillier, S., Tavares, P., and Orlova, E.V. (2007). Structure of bacteriophage SPP1 tail reveals trigger for DNA ejection. EMBO J. *26*, 3720–3728.

Pouillot, F., Blois, H., and Iris, F. (2010). Genetically engineered virulent phage banks in the detection and control of emergent pathogenic bacteria. Biosecur. Bioterror. *8*, 155–169.

Reiss, K., Stencel, J.E., Liu, Y., Blaum, B.S., Reiter, D.M., Feizi, T., Dermody, T.S., and Stehle, T. (2012). The GM2 glycan serves as a functional coreceptor for serotype 1 reovirus. PLoS Pathog. *8*, e1003078.

Ricagno, S., Campanacci, V., Blangy, S., Spinelli, S., Tremblay, D., Moineau, S., Tegoni, M., and Cambillau, C. (2006). Crystal structure of the receptor-binding protein head domain from *Lactococcus lactis* phage bIL170. J. Virol. *80*, 9331–9335.

Schmidt, C. (2019). Phage therapy's latest makeover. Nat. Biotechnol. *37*, 581–586.

Schmidt, T.S.B., Raes, J., and Bork, P. (2018). The human gut microbiome: from association to modulation. Cell *172*, 1198–1215.

Schneider, T.R., and Sheldrick, G.M. (2002). Substructure solution with SHELXD. Acta Crystallogr. D Biol. Crystallogr. *58*, 1772–1779.

Sciara, G., Bebeacua, C., Bron, P., Tremblay, D., Ortiz-Lombardia, M., Lichière, J., van Heel, M., Campanacci, V., Moineau, S., and Cambillau, C. (2010). Structure of lactococcal phage p2 baseplate and its mechanism of activation. Proc. Natl. Acad. Sci. USA *107*, 6852–6857.

Shen, Y., Boulos, S., Sumrall, E., Gerber, B., Julian-Rodero, A., Eugster, M.R., Fieseler, L., Nyström, L., Ebert, M.O., and Loessner, M.J. (2017). Structural and functional diversity in *Listeria* cell wall teichoic acids. J. Biol. Chem. *292*, 17832–17844.

Singh, A.K., Nguyen, T.H., Vidovszky, M.Z., Harrach, B., Benkő, M., Kirwan, A., Joshi, L., Kilcoyne, M., Berbis, M.A., Cañada, F.J., et al. (2018). Structure and N-acetylglucosamine binding of the distal domain of mouse adenovirus 2 fibre. J. Gen. Virol. *99*, 1494–1508.

Söding, J., Biegert, A., and Lupas, A.N. (2005). The HHpred interactive server for protein homology detection and structure prediction. Nucleic Acids Res. *33*, W244–W248.

Spinelli, S., Campanacci, V., Blangy, S., Moineau, S., Tegoni, M., and Cambillau, C. (2006a). Modular structure of the receptor binding proteins of *Lactococcus lactis* phages. The RBP structure of the temperate phage TP901-1. J. Biol. Chem. *281*, 14256–14262.

Spinelli, S., Desmyter, A., Verrips, C.T., de Haard, H.J., Moineau, S., and Cambillau, C. (2006b). Lactococcal bacteriophage p2 receptor-binding protein structure suggests a common ancestor gene with bacterial and mammalian viruses. Nat. Struct. Mol. Biol. *13*, 85–89.

Sumrall, E., Shen, Y., Keller, A., Rismondo, J., Pavlou, M., Eugster, M.R., Boulos, S., Disson, O., Kilcher, S., Wollscheid, B., et al. (2019). Phage resistance at the cost of virulence: *Listeria monocytogenes* serovar 4b requires galactosylated teichoic acids for InlB-mediated invasion. PLoS Pathog. Published online October 7, 2019. https://doi.org/10.1371/journal.ppat.1008032.

Taylor, N.M., Prokhorov, N.S., Guerrero-Ferreira, R.C., Shneider, M.M., Browning, C., Goldie, K.N., Stahlberg, H., and Leiman, P.G. (2016). Structure of the T4 baseplate and its function in triggering sheath contraction. Nature *533*, 346–352.

Terwilliger, T.C., Grosse-Kunstleve, R.W., Afonine, P.V., Moriarty, N.W., Zwart, P.H., Hung, L.W., Read, R.J., and Adams, P.D. (2008). Iterative model building, structure refinement and density modification with the PHENIX AutoBuild wizard. Acta Crystallogr. D Biol. Crystallogr. *64*, 61–69.

Tian, W., Chen, C., Lei, X., Zhao, J., and Liang, J. (2018). CASTp 3.0: computed atlas of surface topography of proteins. Nucleic Acids Res. *46* (*W1*), W363–W367.

Trojet, S.N., Caumont-Sarcos, A., Perrody, E., Comeau, A.M., and Krisch, H.M. (2011). The gp38 adhesins of the T4 superfamily: a complex modular determinant of the phage's host specificity. Genome Biol. Evol. *3*, 674–686.

Uchikawa, K., Sekikawa, I., and Azuma, I. (1986). Structural studies on teichoic acids in cell walls of several serotypes of *Listeria monocytogenes*. J. Biochem. *99*, 315–327.

Veesler, D., Spinelli, S., Mahony, J., Lichière, J., Blangy, S., Bricogne, G., Legrand, P., Ortiz-Lombardia, M., Campanacci, V., van Sinderen, D., and Cambillau, C. (2012). Structure of the phage TP901-1 1.8 MDa baseplate suggests an alternative host adhesion mechanism. Proc. Natl. Acad. Sci. USA *109*, 8954–8958.

Vegge, C.S., Vogensen, F.K., Mc Grath, S., Neve, H., van Sinderen, D., and Brøndsted, L. (2006). Identification of the lower baseplate protein as the antireceptor of the temperate lactococcal bacteriophages TP901-1 and Tuc2009. J. Bacteriol. *188*, 55–63.

Wang, L., Wang, Q., and Reeves, P.R. (2010). The variation of O antigens in gram-negative bacteria. Subcell. Biochem. *53*, 123–152.

Wendlinger, G., Loessner, M.J., and Scherer, S. (1996). Bacteriophage receptors on *Listeria monocytogenes* cells are the N-acetylglucosamine and rhamnose substituents of teichoic acids or the peptidoglycan itself. Microbiology *142*, 985–992.

Winn, M.D., Ballard, C.C., Cowtan, K.D., Dodson, E.J., Emsley, P., Evans, P.R., Keegan, R.M., Krissinel, E.B., Leslie, A.G., McCoy, A., et al. (2011). Overview of the CCP4 suite and current developments. Acta Crystallogr. D Biol. Crystallogr. *67*, 235–242.

Yehl, K., Lemire, S., Yang, A.C., Ando, H., Mimee, M., Torres, M.T., de la Fuente-Nunez, C., and Lu, T.K. (2019). Engineering Phage Host-Range and Suppressing Bacterial Resistance through Phage Tail Fiber Mutagenesis. Cell *179*, 459–469.e9.

Yoichi, M., Abe, M., Miyanaga, K., Unno, H., and Tanji, Y. (2005). Alteration of tail fiber protein gp38 enables T2 phage to infect *Escherichia coli* O157:H7. J. Biotechnol. *115*, 101–107.

Yosef, I., Manor, M., Kiro, R., and Qimron, U. (2015). Temperate and lytic bacteriophages programmed to sensitize and kill antibiotic-resistant bacteria. Proc. Natl. Acad. Sci. USA *112*, 7267–7272.

Yosef, I., Goren, M.G., Globus, R., Molshanski-Mor, S., and Qimron, U. (2017). Extending the host range of bacteriophage particles for DNA transduction. Mol. Cell *66*, 721–728.e3.

Zheng, H., Cooper, D.R., Porebski, P.J., Shabalin, I.G., Handing, K.B., and Minor, W. (2017). CheckMyMetal: a macromolecular metal-binding validation tool. Acta Crystallogr. D Struct. Biol. *73*, 223–233.

Zimmer, M., Sattelberger, E., Inman, R.B., Calendar, R., and Loessner, M.J. (2003). Genome and proteome of *Listeria monocytogenes* phage PSA: an unusual case for programmed + 1 translational frameshifting in structural protein synthesis. Mol. Microbiol. *50*, 303–317.

STAR★METHODS

KEY RESOURCES TABLE

REAGENT or RESOURCE	SOURCE	IDENTIFIER
Bacterial and Virus Strains		
L. monocytogenes EGDe	Internal strain collection, SV1/2a (Shen et al., 2017)	GenBank: NC_003210
L. monocytogenes WSLC1485	Weihenstephan *Listeria* collection, SV3a (Shen et al., 2017)	N/A
L. monocytogenes WSLC1042	Weihenstephan *Listeria* collection, SV4b (Shen et al., 2017)	GenBank: CP007210
L. monocytogenes WSLC1042 Δ*gltB*	Sumrall et al., 2019	N/A
L. monocytogenes WSLC1042 Δ*gttA*	Sumrall et al., 2019	N/A
L. monocytogenes WSLC1042_A511BIM	Sumrall et al., 2019	N/A
L. monocytogenes WSLC1019	Weihenstephan *Listeria* collection, SV4c (Shen et al., 2017)	GenBank: CP013286
L. monocytogenes WSLC1033	Weihenstephan *Listeria* collection, SV4d (Shen et al., 2017)	GenBank: CP013288
L. monocytogenes WSLC3009	Weihenstephan *Listeria* collection, SV5 (Shen et al., 2017)	GenBank: CP007172
L. ivanovii WSLC2011	Weihenstephan *Listeria* collection, SV6a (Shen et al., 2017)	N/A
L. ivanovii WSLC2012	Weihenstephan *Listeria* collection, SV6b (Shen et al., 2017)	N/A
L. seeligeri 4270	SV4a, Soft-cheese isolate, Bavaria, Germany	N/A
L. ivanovii WSLC30151	Weihenstephan *Listeria* collection (Hupfeld et al., 2015)	GenBank: CP009576
Phage PSA	Internal phage collection	GenBank: NC_003291
Phage PSA ΔLCR *ply511*	Kilcher et al., 2018	N/A
Phage PSA ΔLCR *ply511 gp15*_S302R	This study	N/A
Phage PSA ΔLCR *ply511 gp15*_S306K	This study	N/A
Phage PSA ΔLCR *ply511 gp15*_S306R	This study	N/A
Phage PSA ΔLCR *ply511 gp15*_A332V	This study	N/A
Phage PSA ΔLCR *ply511 gp15*_S334R	This study	N/A
Phage PSA ΔLCR *ply511* $gp15_{CO}$_S334R	This study	N/A
Phage PSA ΔLCR *ply511 gp15*_S354T	This study	N/A
Phage PSA ΔLCR *ply511 gp15*_WT $gp15_{CO}$ S334R	This study	N/A
Phage PSA ΔLCR *ply511* stem chimera L99	This study	N/A
Phage PSA ΔLCR *ply511* neck chimera L99	This study	N/A
Phage PSA ΔLCR *ply511* stem chimera ATCC35897	This study	N/A
Phage PSA ΔLCR *ply511* stem chimera WSLC30151	This study	N/A
Phage PSA ΔLCR *ply511* neck chimera WSLC30151	This study	N/A
Chemicals, Peptides, and Recombinant Proteins		
Low Density Nickel	Agarose Bead Technologies	Cat#6BCL-QLNi-X
Critical Commercial Assays		
NEBuilder® HiFi DNA Assembly Master Mix	New England Biolabs	Cat#E2621
Wizard® SV Gel and PCR Clean-Up System	Promega	Cat#A9281
Diversify PCR Random Mutagenesis Kit	Takara	Cat#630703
Phusion High-Fidelity DNA Polymerase	ThermoFisher	Cat#F530L

(*Continued on next page*)

Continued		
REAGENT or RESOURCE	SOURCE	IDENTIFIER
Deposited Data		
Crystal structure of the receptor binding protein (gp15) of *Listeria* phage PSA	This study	PDB: 6R5W
Oligonucleotides		
Primers, see Table S3	Microsynth AG	N/A
Synthetic DNA strings, see Table S3	ThermoFisher	DNA string
Recombinant DNA		
pHGFP PSA gp15 (pQE30 backbone) *ampR*	This study	N/A
pHGFP PSA gp15 CTD (aa210-373) *ampR*	This study	N/A
pHGFP Lm230 RBP CTD *ampR*	This study	N/A
Software and Algorithms		
Prism	Graphpad software Inc.	Version 8 (https://www.graphpad.com/)
Phenix	Adams et al., 2010	Version 1.15.2 (http://www.phenix-online.org/)
XDS	Kabsch, 2010	Version 06/01/2017 (http://xds.mpimf-heidelberg.mpg.de/)
CCP4 package	Winn et al., 2011	Version 7.0 (http://www.ccp4.ac.uk/)
Coot	Emsley et al., 2010	Version 0.8.9.2
PyMol	The Pymol Graphics system	Version 1.4.1 (https://pymol.org/2/)
CLC Genomics Workbench	QIAGEN Bioinformatics	Version 11.0.1 (https://www.qiagenbioinformatics.com/)

LEAD CONTACT AND MATERIALS AVAILABILITY

Further information and requests for resources and reagents should be directed to and will be fulfilled by the Lead Contact, Dr. Samuel Kilcher (samuel.kilcher@hest.ethz.ch). Plasmids and all engineered phages are available upon request.

EXPERIMENTAL MODEL AND SUBJECT DETAILS

Bacterial strains and bacteriophages

E.coli XL-1 blue MRF‘ was cultivated in LB + 15 μg/ml tetracycline at 37°C. All *Listeria* strains were cultivated in 1/2 Brain Heart Infusion (biolife) at 30°C. SVs / WTA architectures of strains EGDe (SV1/2a), WSLC1485 (SV3a), WSLC1042 (SV4b), WSLC1019 (SV4c), WSLC1033 (SV4d), WSLC3009 (SV5), WSLC2011 (SV6a), and WSLC2012 (SV6b) have previously been determined (Shen et al., 2017). *L. seeligeri* 4270 (SV4a) is a serotyped strain isolated from soft cheese in Bavaria, Germany. WSLC30151 (SV5) is a serotyped *L. ivanovii* subspecies *londoniensis* strain (Hupfeld et al., 2015). Phage PSA and its derivatives were propagated on WSLC1042 (PSA WT) or on their new hosts at 30°C using the soft agar overlay method. 10 μL phage dilution and 200 μL stationary host culture were mixed with 4 mL molten LC soft agar (10 g/l typtone, 5 g/l yeast extract, 10 g/l glucose, 7.5 g/l NaCl, 10 mM $CaCl_2$, 10 mM $MgSO_4$, 0.4% agar) at 46°C and poured onto a 1/2 BHI agar plate. Plaque forming units (pfu‘s) were quantified at 24 or 48 h post infection. To quantify multiple phage dilutions, 10 μL phage was spotted onto the solidified soft agar (spot on the lawn assay).

METHOD DETAILS

Protein expression and purification

Plasmid pHGFP (Loessner et al., 2002), a pQE30-derivative (QIAGEN), was used for cloning and production of N-terminal His6- and GFP-tagged full-length (FL) and C-terminal domain (CTD) gp17 constructs (GFP-gp17$_{FL}$ and GFP-gp17$_{CTD}$) in *E. coli* (XL-1 blue MRF‘). FL and CTD gp17were PCR amplified from PSA gDNA and introduced into pHGFP using Gibson assembly (see Table S4). These pHGFP-derived constructs contain an internal TEV cleavage site downstream of the GFP coding sequence, which provided dual functionality for fluorescence cell binding assays and protein crystallization (described below). To express GFP-RBP proteins, 1 l modified LB (15 g/l tryptone, 8 g/l yeast extract, 5 g/l NaCl) was inoculated with the expression strain, grown to OD = 0.5 at 37°C, cooled for 10 min in ice water, induced with 1 mM IPTG (isopropyl-β-d-thiogalactopyranoside), and incubated at 19°C for 16 h. Cells were harvested by centrifugation (7000 x g, 4°C, 15 min), resuspended in 5 mL buffer A (500 mM NaCl, 50 mM Na2HPO4, 5 mM imidazole, 0.1% Tween 20 [pH 8.0]), and disrupted using a Bandelin Sonopuls sonication system (5 min 50% cycle, 80% power). Cell

debris was removed by centrifugation (20'000 x g, 4°C, 45 min) and the crude extract sterile filtered (0.2 μm). Proteins were purified by immobilized metal affinity chromatography using low density nickel chelate beads (agarose bead technologies). Buffer B (500 mM NaCl, 50 mM Na2HPO4, 250 mM imidazole, 0.1% Tween 20 [pH 8.0]) was used for elution, purified proteins were dialyzed against two changes of dialysis buffer (100 mM NaCl, 50 mM NaH2PO4, 0.005% Tween 20 [pH 8.0]), and samples analyzed by SDS-PAGE (Criterion TGX stain-free gel imaged on a BioRad Gel Doc XR+ Molecular Imager).

Cell wall decoration assay

500 μL of a OD-adjusted (OD_{600nm} = 1) stationary phase culture was harvested (5000 g, 4°C, 4 min) and resuspended in 120 μL PBS-T (PBS + 0.1% Tween20). 40 μg GFP-RBP protein was added, incubated on an overhead rotator for 30 min, washed twice with 1 mL PBS-T, and resuspended in 200 μL PBS-T. 150 μL cell suspension was transferred into a black 96-well plate and fluorescence quantified using a FLUOstar Omega microplate reader (excitation: 485 nm; emission: 520 nm). 5 μL of the cell suspension were analyzed using a Leica TCS SPE confocal system equipped with a HCX PL FLUOSTAR 100.0 × 1.30 oil objective.

Phage binding assay

To quantify phage adsorption, 490 μL SM-buffer containing 1 mM $CaCl_2$ were mixed with 10^9 cells of the indicated strain. 10 μL phage dilution containing 10^7 PFU and 500 mL ½ BHI medium were added. Samples were incubated for 20 min at room temperature on an overhead-rotator and subsequently centrifuged (2 min, 4°C, 12'000 x g) to pellet host cells and adsorbed virions. Unbound phage particles were quantified from the supernatant on the wild-type propagation host using the soft-agar overlay method ($PFU_{SUPERNATANT}$). A sample containing 10^7 PFU of phage but no host bacteria was used as input control (PFU_{INPUT}). Relative bound phages were calculated as (PFU_{INPUT}-$PFU_{SUPERNATANT}$)/ PFU_{INPUT}.

Protein crystallization

To provide tag-free $Gp15_{CTD}$, N-terminal His6 and GFP tags were removed from Ni-NTA purified GFP-$gp15_{CTD}$ by TEV protease digestion as previously described (Dunne et al., 2018a). The protein was further purified by anion exchange chromatography with a HiTrap Q HP 5 mL column (GE Healthcare) and eluted using a 0-1 M linear gradient of NaCl in 20 mM Tris, pH 8.0. A single peak eluted around 180mM NaCl containing the $Gp15_{CTD}$ protein, which was collected and dialyzed into 20 mM Tris, pH 7.4. The protein was concentrated to 10 mg/ml for crystallization screening performed in high-throughput 96-well format with sitting-drop vapor-diffusion at 20°C using commercially available screens (Hampton Research, CA, USA; Molecular Dimensions, Suffolk, UK). Tetragonal crystals formed after five days in 0.1 M Na Acetate, pH 4.6, 30% (v/v) PEG 400, and 0.1 M Cadmium Chloride (condition E12, Crystal Screen (Hampton Research, CA, USA)). No optimization was required for subsequent hanging-drop vapor-diffusion crystallization to produce larger crystals, grown at 19°C in hanging drops containing 1 μL protein solution (10 mg/ml) and 1 μL crystallization solution (described above), against a 1 mL reservoir crystallization solution.

Data collection and refinement

A single $Gp15_{CTD}$ crystal was used for native X-ray diffraction data collection on the X06SA (PXI) beamline at the Swiss Light Source, Paul Scherrer Institute, Switzerland, using an Eiger-16M X (DECTRIS Ltd., Baden-Dättwil, Germany) pixel detector at 100 K and wavelength 1.00 Å. A single dataset was collected and automatically indexed, integrated, and scaled using XDS (Kabsch, 2010) in space group $P3_121$ and analyzed using the CCP4 suite (Winn et al., 2011). Despite the high structural similarity predicted by HHpred (Söding et al., 2005) for $Gp15_{CTD}$ to analogous RBPs from Lactococcal phages TP901-1 (PDB ID: 3EJC), p2 (PDB ID: 2BSD) and bil170 (PDB ID: 2FSD), exhaustive molecular replacement attempts using various hybrid assemblies and truncations of RBPs were unsuccessful. Instead, the observation of anomalous signal in the dataset suggested binding of Cadmium atoms from the crystallization condition to the protein. SHELXC/D/E programs (Schneider and Sheldrick, 2002) in the software suite hkl2map (Pape and Schneider, 2004) were used to identify eight heavy atom sites of which six with an occupancy of >0.2 were used to build a poly-alanine model. The initial model was rebuilt with the correct sequence using phenix.autobuild (Terwilliger et al., 2008). Paired refinement using PDB_REDO provided a higher resolution cut-off of 1.70 Å (Joosten et al., 2014). Further rounds of manual model building with COOT (Emsley et al., 2010) and refinement with phenix.refine (Adams et al., 2010) produced a final structure with an R factor of 19.2% (Rfree = 21.1%). The stereochemistry of the model was verified with MolProbity (Chen et al., 2010), which contained 99.8% of residues within favored region of the Ramachandran plot and no residues in disallowed regions. A total of nine Cd^{2+} ions, two polyethylene glycol 400 (PEG 400) chains and two acetate (Ac) groups could be modeled as bound ligands. The CheckMyMetal web server (Zheng et al., 2017) was used to validate and analyze the coordination geometry of all Cd^{2+} ions (Table S6). Oligomerization parameters were analyzed with PDBePISA (Krissinel and Henrick, 2007), structural comparisons performed using the DALI webserver (Holm and Rosenström, 2010) and electrostatic surface potential calculated by APBS (Baker et al., 2001). All structure figures were created using PyMOL (PyMOL Molecular Graphics System, version 1.4.1, Schrodinger LLC). Final model deposited in the Protein Data Bank under Accession Code 6R5W with corresponding crystallographic data collection and refinement statistics provided in Table S7.

Transmission Electron Microscopy of PSA phage particles

Marti et al., 2013PSA was purified from crude phage extracts via PEG precipitation and CsCl ultracentrifugation as previously described (Kilcher et al., 2010) and a high titer (> 10^{10} PFU/ml) phage solution was negatively stained for 30 s with 2% phosphotungstic acid (pH 7.5) onto carbon support films on Cu-400 mesh grids (Quantifoil Micro Tools GmbH, Jena, DE). The samples were observed in a Hitachi HT 7700 (at 100 kV) at the Scientific Center for Optical and Electron Microscopy (ScopeM) facility, ETH Zurich.

Phage genome assembly and activation by transfection into Listeria L-forms

In vitro assembly of synthetic genomes was performed as previously described (Kilcher et al., 2018). Briefly, genomes were partitioned into multiple DNA fragments that feature 40 nt overlaps with their neighboring fragments. DNA was amplified from purified phage DNA (or ligated phage gDNA for the amplification of fragments spanning the PSA cos-site) using Phusion DNA polymerase (Thermo Scientific). Annealing temperatures were calculated using the ThermoFisher Tm calculator and extension times were determined based on an assumed polymerase speed of 45 s/kb. Equimolar amounts (0.03 pmol) of purified fragments were employed to assemble synthetic genomes using the Gibson method (NEBuilder HiFi DNA Assembly Cloning Kit, New England Biolabs; 1h at 50°C). Rev2L L-forms were inoculated in 1 mL modified DM3 medium (5 g/l yeast extract, 5 g/l tryptone, 0.01% BSA, 500 mM succinic acid, 5 g/l glucose, 20 mM K_2HPO_4, 11 mM KH_2PO_4, 20 mM $MgCl_2$, pH 7.3) and grown for 96 h at 32°C. L-forms were suspended by pipetting, adjusted to OD_{600nm} = 0.15 using DM3, and transformed with 15 mL of the genome assembly reaction: 100 μL OD-adjusted L-forms were mixed with DNA in a 50 mL Falcon tube and 150 μL polyethylene-glycol solution (PEG average molecular weight: 20‘000 g/mol) was added and thoroughly suspended. After 5 min, 10 mL pre-warmed DM3 medium was added and suspended, and the transformation reaction incubated at 32°C for 24 h. Transfection reactions were assayed for produced synthetic phages using the soft-agar overlay method (typically using 50-500 μL transformation reaction per overlay). Primers, PCR reactions, and synthetic DNA strings used for the construction of the PSA ΔLCR ply511-derived chimeras are listed in Tables S3 and S4. The RBP genes of all isolated synthetic phages were validated by PCR and Sanger sequencing (Microsynth AG, Balgach, Switzerland).

RBP diversification

The diversified RBP fragments were generated by epPCR using the Diversify PCR Random Mutagenesis Kit (Clontech) according to the manufacturers instructions. Reactions were set up to produce 2.0 (40 μM dGTP), 3.5 (480 μM $MnSO_4$, 40 μM dGTP), and 5.8 (640 μM $MnSO_4$, 120 μM dGTP) mutations per kilobase, the resulting PCR fragments were purified, mixed at equimolar ratios, and used for assembly of synthetic phage genome libraries. The corresponding synthetic phage library was produced as described above. PCR reactions and primers used for the construction of the PSA ΔLCR ply511 RBP library are listed in Tables S3 and S4.

Identification of prophage-encoded Gp15-like RBPs

To identify potential RBPs that are compatible with the modular architecture of Gp15, particularly with the segmented coiled coil of the Gp15 stem and neck, a protein blast search was performed using the Gp15 stem and neck (aa 202-259) as query sequence. We focused on genes from *Listeria* strains with annotated SVs and identified 20 RBP candidates that fit these criteria, spanning SVs 1/2 (12 lysogens), 4a (1 lysogen), 4b (5 lysogens), 5 (1 lysogen), and 6b (1 lysogen) (Table S2). Gp15-like candidates from non-*Listeria* hosts are shown in Table S5.

Bioinformatics

Multiple sequence alignments of full-length RBPs, neck-, and head domains were constructed using CLC Genomics Workbench 11.0 (QIAGEN; settings: gap open cost = 10; gap extension cost = 1; endgap cost = cheap). Phylogenetic trees of RBP head domains were also constructed using CLC Genomics Workbench (settings: algorithm = neighbor joining; distance measure = Jukes-Cantor; bootstrapping = 100 replicates). *Listeria* head-domain candidates were identified by protein blast search (Altschul et al., 1990) against published *Listeria* genomes (taxid:1637) using the PSA neck domain (aa 197-251) as query sequence and all hits were manually inspected for SV annotation.

QUANTIFICATION AND STATISTICAL ANALYSIS

Data on all graphs was obtained from three independent experiments and show the mean with the error bars representing SD; n = number of independent replicates. Statistical significance was calculated with the Prism software (Graphpad software Inc, version 8) using Student‘s t test. In all figures: ns = not significant; * = p value < 0.05; ** = p value < 0.01; *** = p value < 0.001; **** = p value < 0.0001.

DATA AND CODE AVAILABILITY

The Protein Data Bank accession code for the crystal structure of the receptor binding protein (Gp15) of *Listeria* phage PSA is PDB: 6R5W.

Cell Reports, Volume *29*

Supplemental Information

Reprogramming Bacteriophage Host Range through Structure-Guided Design of Chimeric Receptor Binding Proteins

Matthew Dunne, Beatrice Rupf, Marc Tala, Xhem Qabrati, Patrick Ernst, Yang Shen, Eric Sumrall, Laura Heeb, Andreas Plückthun, Martin J. Loessner, and Samuel Kilcher

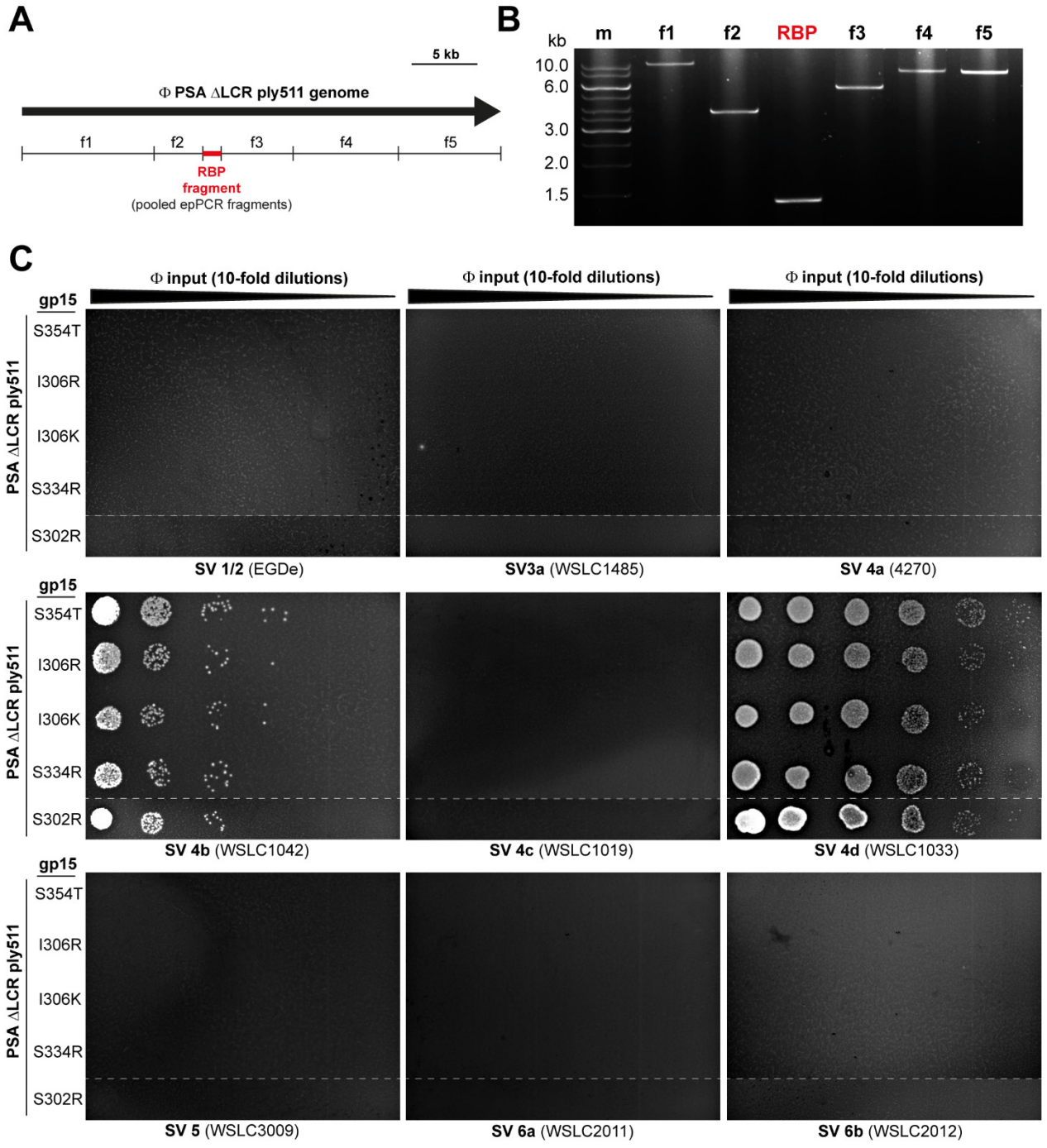

Figure S1, related to Figure 2: (**A-B**) Design and amplification of genome fragments for the construction of randomized RBP phage library. (**A**) Overlapping fragments f1 – f5 were amplified using a high fidelity polymerase, whereas the RBP fragment was amplified by error-prone PCR using primers P11 and P12 (see also **Tables S3 and S4**). (**B**) All fragments were purified and analyzed by agarose gel electrophoresis. (**C**) Host ranges of PSA ΔLCR *ply511*-derived RBP point mutants. Plating efficiencies of all isolated RBP point mutants were determined on representative strains of the major *Listeria* SVs using spot on the lawn assays. Plaque formation was restricted to SVs 4b and 4d.

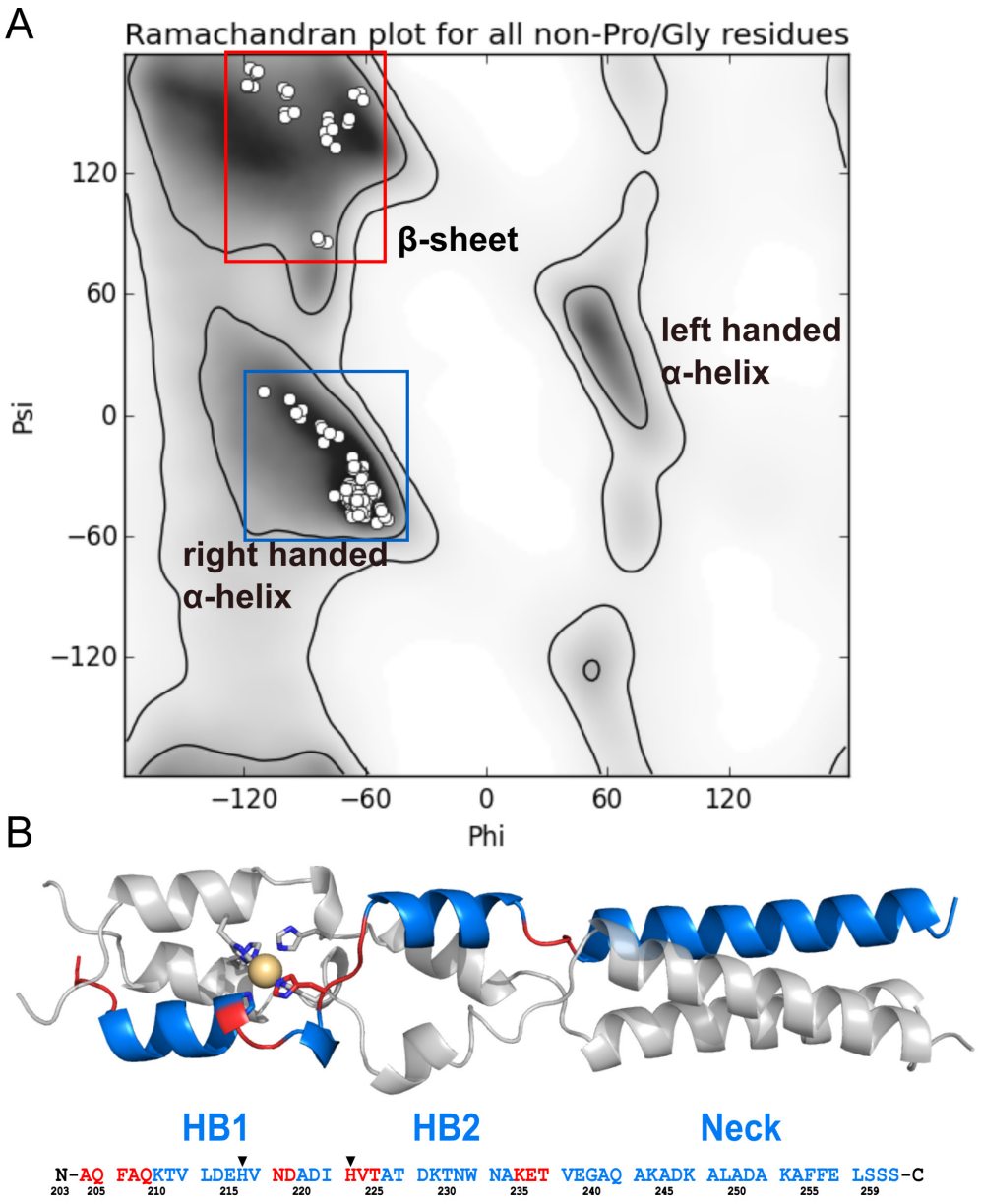

Figure S2, related to Figure 4. Conformational analysis of connecting β-layers and their segmentation of the stem and neck domains. (**A**) Ramachandran plot generated by MolProbity (Chen et al., 2010) of the backbone torsion angles for the stem and neck domains. All residues within helical bundles HB1 and HB2 and 3_{10} helix (blue box) have dihedral angles resembling those of right handed α-helices, whereas all residues within the interconnecting β-layers (red box) have dihedral angles resembling β-sheets (i.e., ϕ = -60 to -120º and ψ = 80 to 180º), as described in detail for this supersecondary structure (Hartmann, 2017). (**B**) Ribbon diagram and corresponding amino acid sequence for the stem and neck domains of gp15 with connecting β-layers and coiled coil α-helices colored red and blue, respectively. Connecting HB1 to HB2 is a 10-residue β-layer featuring the central 3_{10} helix. The shorter 3-residue β-layer connects the end of HB2 to the coiled coil neck domain. At the interface of HB1 and the connecting β-layer is a metal binding site (brown sphere; Cd^{2+}_{stem}) positioned in the center of the three-fold axis of the RBP, octahedrally coordinated by the side-chain Nε2 groups (shown as sticks) of His214 and His221 residues of all three monomers.

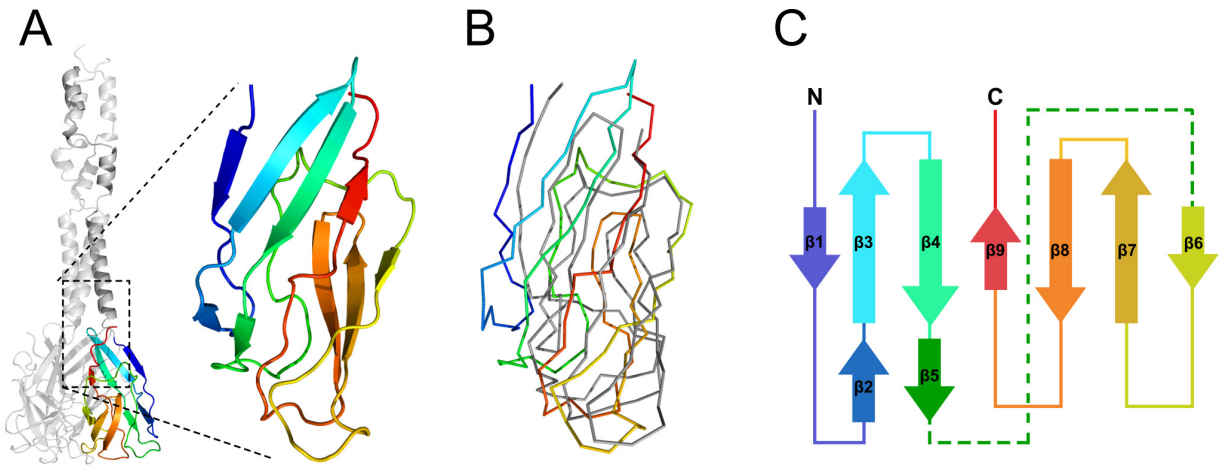

Figure S3, related to Figure 5. (**A**) Ribbon diagram of the $gp15_{CTD}$ homotrimer with a single head domain colored from N-terminus (blue) to C-terminus (red) and highlighted. **B)** Superposition of the gp15 head domain (rainbow) with TP901-1 (PDB ID: 3EJC; shown in grey) and P2 (PDB ID: 2BSD; not shown) yielded rmsd values of 3.2 Å for 130 residues and 3.7 Å for 119 residues, respectively. **C)** Topology diagram with secondary structure β-Strands shown as arrows of a single head domain reveals the quasi-double Greek key motif conserved across various viral head domains (as shown in Fig. 5).

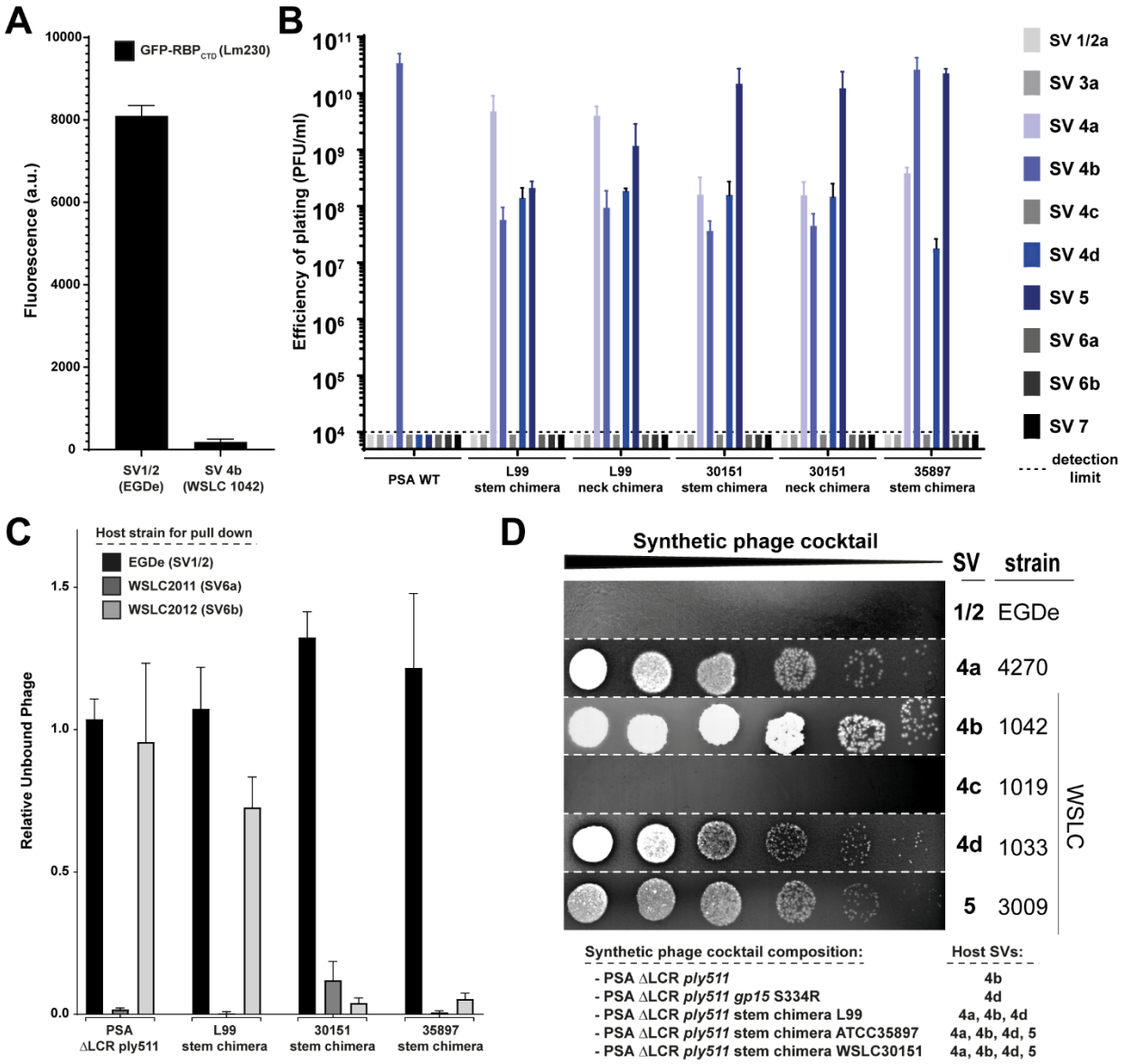

Figure S4, related to Figure 6: (**A**) The RBP candidate identified in strain Lm230 has predicted SV 1/2-specificity: Spectrofluorometric binding assays using a purified GFP-RBP$_{CTD}$ protein derived from the putative Lm230-encoded RBP reveals specific decoration of SV1/2 cells. Even though stem and neck chimeras with Lm230-derived head domains did not produce plaques on any SV, this data proofs the predicted RBP binding-specificity. (**B**) Plating efficiencies of PSA ΔLCR *ply511* and chimeric PSA derivatives on a panel of *Listeria* strains with divergent WTA architectures. Plating efficiencies of PSA ΔLCR *ply511* and the indicated chimeric phages were determined using spot on the lawn assays on *Listeria* strains covering SV 1/2 (strain EGDe), SV 3a (WSLC 1485), SV 4a (4270), SV 4b (WSLC 1042), SV 4c (WSLC 1019), SV 4d (WSLC 1033), SV 5 (WSLC 3009), SV 6a (WSLC 2011), and SV 6b (WSLC 2012). (**C**) Phage binding assays were performed using PSA ΔLCR *ply511* and the indicated PSA ΔLCR *ply511*-derived chimeric phages to quantify adsorption to SV 1/2 (strain EGDe, black bars), SV 6a (WSLC 2011, dark grey), and SV 6b cells (WSLC 2012, light grey), on which no plaque formation was observed. SVs 6b and SV 5 share identical RboP repeating units. SV 6a and SV 4b both feature galactosylated GlcNAc at the RboP C2 position, which is the receptor epitope of WT Gp15. Graph shows unbound phage particles relative to a phage only control. (**D**) PSA-based phage cocktail controls most *Listeria* serovars that feature typeII WTA. A phage cocktail was prepared containing equal titers of the indicated PSA-derivatives. 10-fold dilutions of the resulting phage cocktail were spotted on representative *Listeria* serovars covering both typeI (EGDe) and typeII WTAs (all other). All data is mean ± SD from three independent experiments.